Article

Caveolin-1 is ubiquitinated and targeted to intralumenal vesicles in endolysosomes for degradation

HAYER, Arnold, *et al*.

Abstract

Caveolae are long-lived plasma membrane microdomains composed of caveolins, cavins, and a cholesterol-rich membrane. Little is known about how caveolae disassemble and how their coat components are degraded. We studied the degradation of caveolin-1 (CAV1), a major caveolar protein, in CV1 cells. CAV1 was degraded very slowly, but turnover could be accelerated by compromising caveolae assembly. Now, CAV1 became detectable in late endosomes (LE) and lysosomes where it was degraded. Targeting to the degradative pathway required ubiquitination and the endosomal sorting complex required for transport (ESCRT) machinery for inclusion into intralumenal vesicles in endosomes. A dual-tag strategy allowed us to monitor exposure of CAV1 to the acidic lumen of individual, maturing LE in living cells. Importantly, we found that "caveosomes," previously described by our group as independent organelles distinct from endosomes, actually correspond to late endosomal compartments modified by the accumulation of overexpressed CAV1 awaiting degradation. The findings led us to a revised model for endocytic trafficking of CAV1.

Reference

HAYER, Arnold, *et al*. Caveolin-1 is ubiquitinated and targeted to intralumenal vesicles in endolysosomes for degradation. *The Journal of Cell Biology*, 2010, vol. 191, no. 3, p. 615-629

DOI : 10.1083/jcb.201003086
PMID : 21041450

Published November 1, 2010

Caveolin-1 is ubiquitinated and targeted to intralumenal vesicles in endolysosomes for degradation

Arnold Hayer, Miriam Stoeber, Danilo Ritz, Sabrina Engel, Hemmo H. Meyer, and Ari Helenius

Institute of Biochemistry, ETH Zurich, 8093 Zurich, Switzerland

Caveolae are long-lived plasma membrane microdomains composed of caveolins, cavins, and a cholesterol-rich membrane. Little is known about how caveolae disassemble and how their coat components are degraded. We studied the degradation of caveolin-1 (CAV1), a major caveolar protein, in CV1 cells. CAV1 was degraded very slowly, but turnover could be accelerated by compromising caveolae assembly. Now, CAV1 became detectable in late endosomes (LE) and lysosomes where it was degraded. Targeting to the degradative pathway required ubiquitination and the endosomal sorting complex required for transport (ESCRT) machinery for inclusion into intralumenal vesicles in endosomes. A dual-tag strategy allowed us to monitor exposure of CAV1 to the acidic lumen of individual, maturing LE in living cells. Importantly, we found that "caveosomes," previously described by our group as independent organelles distinct from endosomes, actually correspond to late endosomal compartments modified by the accumulation of overexpressed CAV1 awaiting degradation. The findings led us to a revised model for endocytic trafficking of CAV1.

Introduction

Caveolae are small plasma membrane invaginations in the surface of many mammalian cell types. They are implicated in various physiological processes including endo- and transcytosis, pathogen entry, lipid regulation, signaling, and cancer (Razani et al., 2002; Parat, 2009). They can bud into the cell in the form of endocytic vesicles that dock onto endosomal organelles for cargo delivery (Pelkmans et al., 2004; Parton and Simons, 2007). In the plasma membrane and during the vesicular transport cycle, the caveolar coat remains tightly associated with the membrane, in striking contrast to other vesicle coats such as clathrin or COPI/II (Tagawa et al., 2005).

The caveolar coat is composed of two major layers of protein. The inner layer in nonmuscle cells is composed of CAV1 (caveolin-1) and CAV2. The caveolins are integral membrane proteins with a central hydrophobic domain inserted as a loop inside the membrane. With both N and C termini facing the cytoplasm, CAV1 assumes a hairpin topology (Dupree et al., 1993; Monier et al., 1995). With CAV1 as the major organizing subunit, the two caveolins form an interconnected scaffold that defines the size and many of the overall properties of the microdomain. The recently discovered cavins provide an outer peripheral cytosolic protein layer. They constitute large, heteroligomeric complexes that cover the highly curved membrane of plasma membrane caveolae (Bastiani et al., 2009; McMahon et al., 2009; Hayer et al., 2010). They are thought to stabilize the caveolin scaffold, promote membrane curvature, and regulate budding of caveolae (Hill et al., 2008; Liu and Pilch, 2008; Bastiani et al., 2009; Hansen et al., 2009; McMahon et al., 2009). The lipid bilayer associated with caveolae represents a specialized microdomain enriched in cholesterol and sphingolipids.

Caveolins are synthesized in the ER, where they rapidly form SDS-resistant 8S oligomers containing 7–10 CAV1 and

Correspondence to Ari Helenius: ari.helenius@bc.biol.ethz.ch

A. Hayer's present address is Dept. of Chemical and Systems Biology, Stanford University Medical Center, Stanford, CA 94305.

H.H. Meyer's present address is Molecular Biology Laboratory, Faculty of Biology, Centre of Medical Biotechnology, University of Duisburg-Essen, 45117 Essen, Germany.

Abbreviations used in this paper: BafA, bafilomycin A_1; EE, early endosomes; ESCRT, endosomal sorting complex required for transport; FA, formaldehyde; ILV, intralumenal vesicles; LE, late endosomes; LYS, lysosomes; mCherry, monomeric Cherry; mEGFP, monomeric EGFP; mRFP, monomeric RFP; TIR, total internal reflection; TIR-FM, TIR fluorescence microscopy.

Supplemental Material can be found at:
http://jcb.rupress.org/content/suppl/2010/10/29/jcb.201003086.DC1.html
Original image data can be found at:
http://jcb-dataviewer.rupress.org/jcb/browse/3502

The Rockefeller University Press $30.00
J. Cell Biol. Vol. 191 No. 3 615–629
www.jcb.org/cgi/doi/10.1083/jcb.201003086

Published November 1, 2010

CAV2 molecules (Scheiffele et al., 1998; Fernandez et al., 2002; Hayer et al., 2010). After COPII-dependent transport to the Golgi complex, the 8S oligomers associate with cholesterol and with each other to form the aforementioned membrane-embedded scaffold composed of 15–25 8S complexes. The scaffolds sediment as 70S particles when extracted from the membrane and delipidated (Hayer et al., 2010). A special vesicular pathway is responsible for transporting the caveolin scaffolds to the plasma membrane, where the cavins associate with them in the form of large 60S complexes (Hayer et al., 2010).

Once properly formed, caveolae in the plasma membrane are stable structures in which neither the caveolins nor the cavins undergo rapid turnover. They can be activated and undergo endocytic internalization (Kirkham et al., 2005; Tagawa et al., 2005), and there is evidence that they can participate in cycles of fusion and fission with the plasma membrane (Pelkmans and Zerial, 2005). Cholesterol is not only needed for assembly of caveolae but also for stability (Rothberg et al., 1992). Cavins also contribute to the stability of caveolae as down-regulation of cavin-1 shortens the half-life of CAV1 (Hill et al., 2008; Hansen et al., 2009). Because the degradation of CAV1 after cavin-1 down-regulation is sensitive to lysosomal inhibitors, it is possible that it occurs in lysosomes (LYS; Hill et al., 2008). However, it has been reported that mutants of CAV1 that fail to assemble into caveolae and thus remain trapped in the Golgi, and CAV2 expressed in the absence of CAV1, are degraded by a proteasomal pathway (Galbiati et al., 2000; Razani et al., 2001).

In this study, we address the processes by which caveolae and CAV1 undergo assembly, disassembly, and especially degradation. By altering the balance of the different components of caveolae in the cell (CAV1, cavin-1, and cholesterol), we could inhibit caveolae assembly, thereby accelerating CAV1 degradation. Thus, the unassembled CAV1 generated was targeted to endosomes, ubiquitinated, sequestered in intralumenal vesicles (ILV) by the endosomal sorting complex required for transport (ESCRT) machinery, and degraded in LYS. The vacuoles previously described as caveosomes could be identified as late endosomes (LE) and LYS (LE/LYS) enriched in CAV1 destined for degradation.

Results

Unassembled caveolin in the plasma membrane

To learn more about the life cycle of caveolae and about CAV1 degradation, we analyzed the consequences of perturbing the ratios and availability of caveolar components in CV1 cells. Manipulation was performed in three ways, depleting cells of cholesterol, overexpressing CAV1, and knocking down cavin-1 expression.

Cholesterol depletion was performed in CV1 cells stably expressing CAV1–monomeric EGFP (mEGFP). This cell line produced CAV1-mEGFP homogenously at levels similar to that of endogenous CAV1, resulting in moderate overexpression (Fig. S1 A). By fluorescence microscopy, CAV1-mEGFP was observed as familiar, subresolution spots in the plasma membrane corresponding to caveolae (Fig. 1 A) and as a diffuse staining of the Golgi complex.

To lower the level of cholesterol in the plasma membrane and the Golgi complex, we used U18666A, an amphiphilic amine that inhibits cholesterol synthesis and perturbs cholesterol trafficking. It induces cholesterol accumulation in swollen LE/LYS, thereby depleting cholesterol elsewhere (Cubells et al., 2007). The CAV1-mEGFP in the plasma membrane of U18666A-treated CV1 cells was predominantly uniformly distributed with only few defined spots characteristic of caveolae (Fig. 1 B). Consistent with the lack of caveolae, FRAP analysis showed that the CAV1-mEGFP in the plasma membrane was significantly more mobile than in untreated cells (Fig. 1 C). Under normal conditions, caveolae are stable and immobile unless activated (Thomsen et al., 2002; Tagawa et al., 2005).

Did the unassembled CAV1 originate from plasma membrane caveolae or from a defect in caveolae assembly? We undertook total internal reflection (TIR) fluorescence microscopy (TIR-FM) in live cells to discriminate between these possibilities. In control cells, caveolar scaffolds arrive at the plasma membrane from the Golgi in preassembled form in vesicular carriers distinct from those used by most other membrane cargo (Tagawa et al., 2005; Hayer et al., 2010). When vesicles fuse with the plasma membrane, the CAV1 does not diffuse away but persists as immobile, tight spots. That the CAV1-mEGFP transport was different in CV1 cells pretreated with U18666A was shown by two observations. First, the CAV1-mEGFP was delivered to the cell surface in tubular rather than small vesicular carriers (Fig. 1 D and Video 1; Tagawa et al., 2005). Such tubular carriers are typical of the constitutive pathway of transport from the Golgi to the plasma membrane (Toomre et al., 1999). Second, the CAV1-mEGFP rapidly dispersed from the site of vesicle fusion laterally into the surrounding plasma membrane (Fig. 1 D and Video 1). This suggested that it arrived in unassembled or easily dissociated form. The most likely explanation for the diffuse plasma membrane staining was that by depleting cholesterol, the assembly of intact caveolin scaffolds was inhibited in the Golgi complex. Apparently, the unassembled or incompletely assembled CAV1 was transported to the surface via a constitutive vesicle transport pathway and not by the alternative pathway normally used by caveolar scaffolds (Hayer et al., 2010). Although it was not obvious in the TIR-FM videos, it was possible that disassembly of caveolae at the plasma membrane could contribute to the phenotype. We have previously shown loss of caveolar spots and a rise in diffuse CAV1 staining when cholesterol is removed from the plasma membrane using methyl-β-cyclodextrin (Tagawa et al., 2005).

In addition to the diffuse plasma membrane staining of CAV1 in U18666A-treated cells, CAV1 was found in some of the large, swollen cytoplasmic organelles that the inhibitor induced in cells. Confocal microscopy showed that these were positive for the late endosomal/lysosomal marker Lamp1 (Fig. 1, E and F). They were scattered around the cytoplasm and had the appearance of caveosomes as described in CAV1-EGFP–expressing cells (Pelkmans et al., 2001).

The effects of CAV1 overexpression and cavin-1 silencing

Overexpression of CAV1-mEGFP induced by transient transfection provided another perturbation with similar effects on

Published November 1, 2010

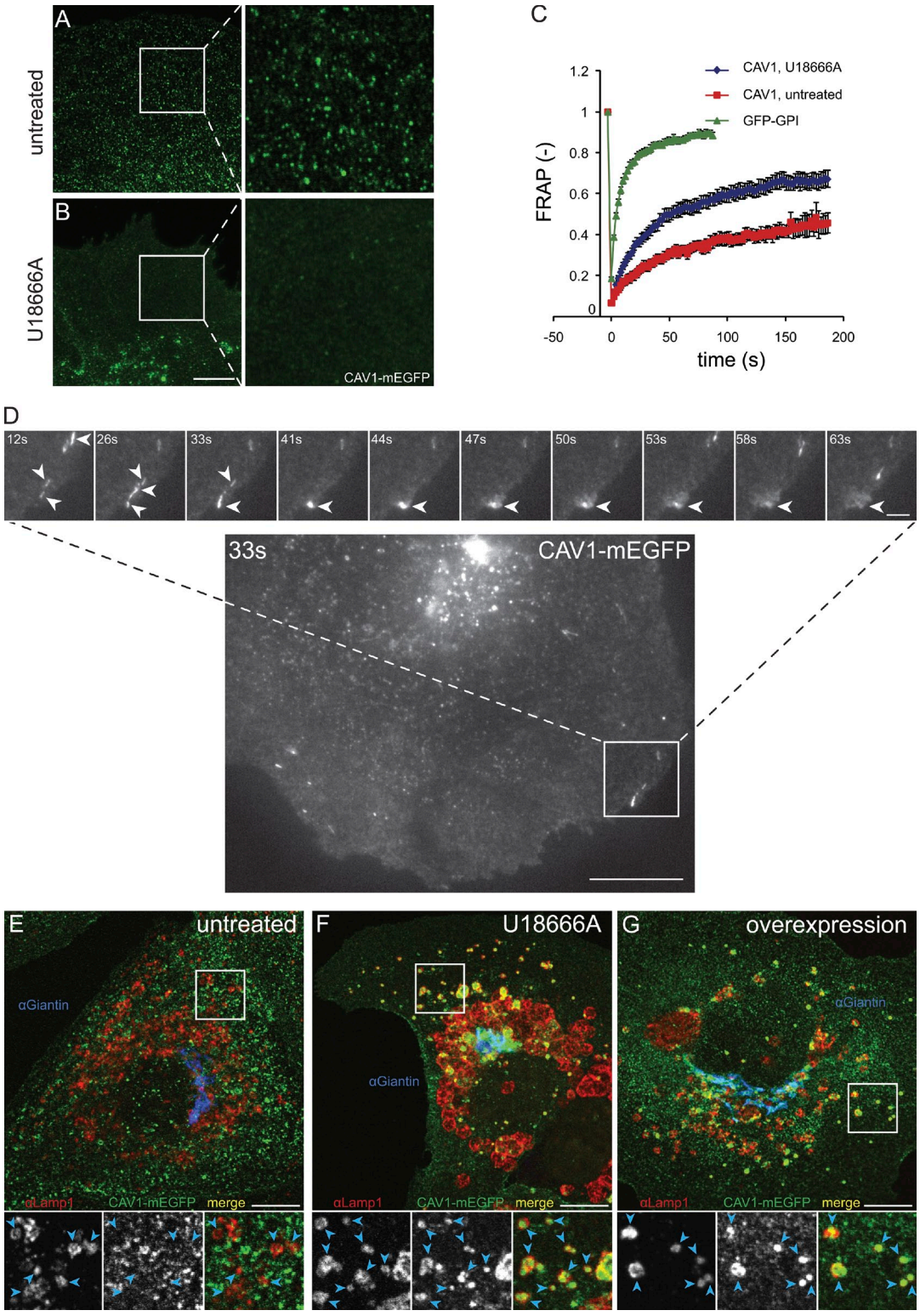

Figure 1. **Unassembled caveolin in the plasma membrane.** (A and B) CV1-CAV1-mEGFP cells were left untreated (A) or treated with 5 µg/ml U18666A for 16 h (B), fixed, and viewed by confocal microscopy. U18666A treatment resulted in a noncaveolar pool of CAV1 in the plasma membrane. (right) Insets show enlargements of the boxed areas. (C) FRAP analysis of the noncaveolar surface pool of CAV1. 4 × 4–µm squares were photobleached in the periphery of either CV1-CAV1-mEGFP cells (5 µg/ml U18666A treated for 16 h [n = 10 cells]; and untreated [n = 5 cells]) or a CV1 cell line stably expressing GFP-GPI (n = 15 cells). Error bars indicate mean ± SEM. (D) CV1 cells pretreated with 5 µg/ml U18666A (16 h) were transfected with CAV1-mEGFP and post-Golgi trafficking imaged by TIR-FM time-lapse imaging (1 Hz). The evanescent field was adjusted such that the plasma membrane and part of the Golgi were illuminated. Tubular carriers arriving at the surface and releasing CAV1-mEGFP upon fusion with the plasma membrane are seen. Note that CAV1-mEGFP diffused laterally, and no caveolar spots were left behind (see Video 1). (top) Insets show enlargements of the boxed area. (E–G) Treating CV1-CAV1-mEGFP cells with 5 µg/ml U18666A (16 h) or overexpressing CAV1-mEGFP in CV1 cells (16 h) induced unassembled CAV1 in the plasma membrane and targeting of CAV1-mEGFP to Lamp1-positive LE (single confocal sections). (bottom) Insets show enlargements of the corresponding boxed areas. Arrowheads point to Lamp1-positive LE, indicating absence (E) or presence (F and G) of colocalization with CAV1-mEGFP. Bars: (B, D [bottom], and E–G) 10 µm; (D [top]) 2 µm.

Published November 1, 2010

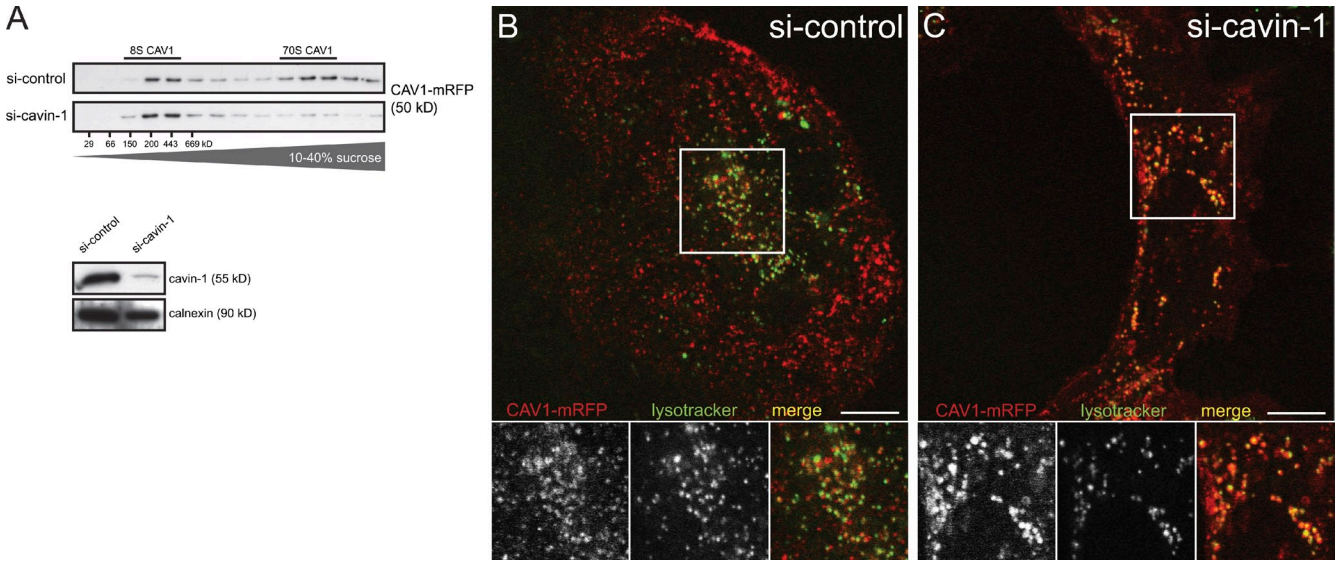

Figure 2. **Cavin-1 knockdown.** (A) Cavin-1 knockdown in HeLa-CAV1-mRFP cells caused an almost complete redistribution of assembled 70S-CAV1 into unassembled 8S-CAV1 as determined by sucrose velocity gradient centrifugation. (B and C) HeLa-CAV1-mRFP cells treated with control siRNA (B) or siRNA targeting cavin-1 (C) were loaded with 100 nM LysoTracker (green) for 1 h and imaged live by confocal microscopy. Cavin-1 knockdown caused loss of caveolar spots in the plasma membrane and accumulation of CAV1-mRFP in acidic, LysoTracker-positive organelles. (B and C, bottom) Insets show enlargements of boxed areas. Blots and images are representative of at least three independent experiments. Bars, 10 µm.

caveolae assembly and CAV1 distribution in the cell. When CAV1-mEGFP was transiently overexpressed and allowed to accumulate over 16 h in CV1 cells, the distribution of CAV1 showed, in addition to a uniform fluorescence in the plasma membrane, accumulation of label in the Golgi complex and in Lamp1-positive LE/LYS (Fig. 1 G). Co-overexpression of cavin-1 with CAV1 did not reverse this effect (Fig. S1 C).

It is important to note that a few hours after transfection with CAV1 constructs, most of the expressed CAV1 was already localized to the noncaveolar surface pool and to endosomal organelles; i.e., their localization differed from that observed for endogenous CAV1 in control cells. Transiently overexpressed CAV1 was therefore not a suitable marker for caveolae beyond a certain time of expression. The extent of mislocalization also depended on cell type and transfection method. For example, after transfection by electroporation or lipid-based transfection methods (see Materials and methods), expression for 4–5 h was enough to show mislocalization in CV1 cells. When expression of CAV1 constructs was necessary, as it was in the visualization of CAV1 in live cells, it was better to use cell lines stably expressing the CAV1 constructs. The expression level was lower, and the CAV1 distribution generally mirrored that observed for endogenous CAV1 in control cells.

The third manipulation of CAV1 assembly involved cavin-1, another essential caveolar coat component. Because knockdown of cavin-1 by siRNA causes concomitant down-regulation of endogenous CAV1 (Hill et al., 2008; Hansen et al., 2009; Hayer et al., 2010), an siRNA that targeted cavin-1 was transfected into HeLa cells stably expressing CAV1–monomeric RFP (mRFP; HeLa-CAV1-mRFP). This resulted in efficient knockdown of cavin-1 with only partial loss of CAV1-mRFP expression (Fig. 2 A). CAV1-mRFP was now present as a uniform pool in the plasma membrane and in cytoplasmic vacuoles that could be stained with LysoTracker, a marker for LE/LYS (Fig. 2, B and C). Furthermore, sucrose velocity gradient centrifugation of HeLa-CAV1-mRFP extracts showed that cavin-1 knockdown resulted in an almost complete loss of the 70S CAV1 complexes, which is consistent with the observed redistribution of CAV1-mRFP from a caveolar to a noncaveolar surface pool composed of 8S complexes (Fig. 2 A). Apparently, the CAV1 in the vacuoles was also present as 8S complexes. Because cavin-1 is not needed for assembly of the caveolin scaffold in the Golgi complex (Hayer et al., 2010), the effect of cavin-1 knockdown was most likely explained by instability of assembled caveolar scaffolds in the absence of cavins.

Collectively, the results indicated that interfering with the assembly of caveolae resulted in the appearance of an unassembled, rapidly diffusing pool of caveolins in the plasma membrane, probably representing 8S complexes. Furthermore, CAV1 accumulated in LE/LYS, where it was not detectable under normal conditions. Cholesterol depletion, CAV1 overexpression, and silencing of cavin-1 all had similar effects.

Acidification is required for CAV1 degradation

To determine the half-life of CAV1, we used metabolic labeling with [^{35}S]Cys/Met and a pulse-chase approach. The amount of labeled CAV1 was determined at different times of chase using immunoprecipitation with the anti-CAV1 (N20) antibody, SDS-PAGE, and autoradiography. Under normal conditions, the endogenous CAV1 proved to be an extremely long-lived protein in CV1 and HeLa cells. The half-life was much longer than 36 h (Fig. 3 A and not depicted). This was consistent with the stability demonstrated for caveolar domains in the plasma membrane of cells (Thomsen et al., 2002; Tagawa et al., 2005). However, transiently overexpressed CAV1-HA was degraded at a much higher rate, and we could estimate its half-life to 13.6 h (Fig. 3 A).

Published November 1, 2010

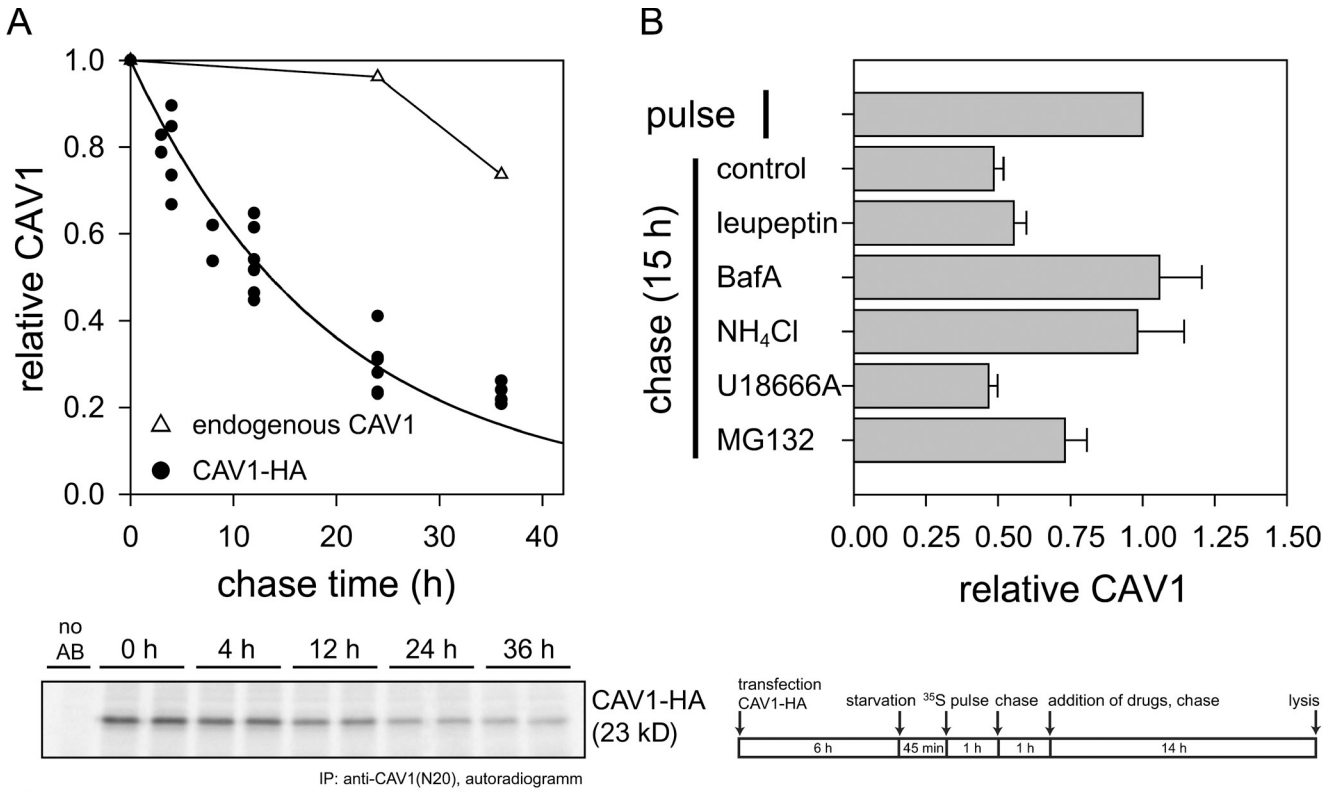

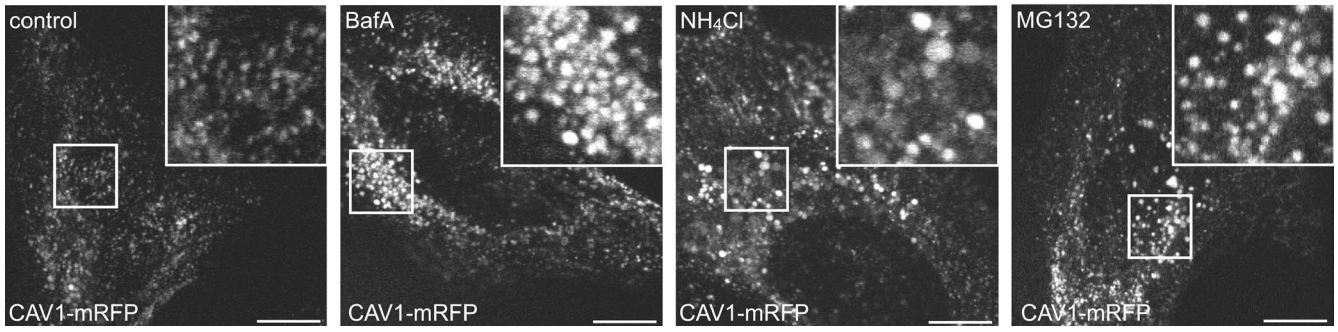

Figure 3. **CAV1 degradation requires endosomal acidification.** (A) Degradation time course of endogenous CAV1 and transiently transfected CAV1-HA in CV1 cells as determined by a pulse-chase experiment (see Materials and methods). $t_{1/2}$ of CAV1-HA was 13.6 h, as determined by an exponential fit to data points from $n = 3$ independent experiments. Endogenous CAV1 was degraded much slower ($t_{1/2}$ >36 h). (B) Degradation of CAV1-HA was inhibited by 0.2 µM BafA and 20 mM NH_4Cl, which neutralize endosomal acidification, and by 10 µM MG132, an inhibitor of the ubiquitin–proteasome system. Error bars indicate mean ± SEM ($n = 3$–5 independent experiments). (C) Treatment of HeLa-CAV1-mRFP cells with BafA, NH_4Cl, or MG132 caused accumulation of CAV1-mRFP in endosomal organelles. Single confocal sections of living cells, focus set to perinuclear endosomes. Insets show enlargements of boxed areas. Bars, 10 µm.

The shorter half-life of overexpressed CAV1-HA allowed us to study the pathway of degradation using inhibitors. The degradation of CAV1-HA was completely inhibited by bafilomycin A_1 (BafA) and NH_4Cl, which inhibit lysosomal degradation by raising the lumenal pH (Fig. 3 B). The proteasomal inhibitor MG132 had a partial effect, which is consistent with an indirect role described for proteasomes in endosome maturation and the lysosomal degradation of the EGF receptor (Longva et al., 2002). U18666A and leupeptin had little or no effect on degradation. Consistent with the inhibitor profile, HeLa cells stably expressing CAV1-mRFP and treated with BafA, NH_4Cl, or MG132 showed increased accumulation of CAV1-mRFP in endosomal structures relative to control cells (Fig. 3 C). Together, these data indicated that CAV1 was targeted to LYS for degradation. This also occurred in the stably expressing cells with a normal intracellular CAV1 distribution and only mildly overexpressing CAV1-mRFP (Fig. S1 B).

CAV1 in the endo/lysosomal pathway

When CAV1–monomeric Cherry (mCherry) was transiently coexpressed in CV1 cells with EGFP-tagged Rab5, Rab7, or Lamp1, colocalization was observed in cytoplasmic vacuoles using confocal fluorescence microscopy in fixed and live cells (Fig. 4, A–C). We undertook quantitative colocalization analysis based on images acquired from live cells coexpressing CAV1-mCherry and a GFP-tagged endosomal marker. Altogether, ~6×10^4 endosomes

Published November 1, 2010

were analyzed from cells expressing CAV1-mCherry/EGFP-Rab5 (n = 68), CAV1-mCherry/EGFP-Rab7 (n = 68), and CAV1-mCherry/Lamp1-EGFP (n = 43). The results showed that of the CAV1-mCherry–positive endosomal structures, 27% colocalized with EGFP-Rab5, 61% with EGFP-Rab7, and 67% with Lamp1-EGFP (Fig. 4 G and Fig. S2 A). In live cells, CAV1-mCherry colocalized with EGFP-Rab5 in the limiting membrane of early endosomes (EE), whereas in LE/LYS positive for EGFP-Rab7 or Lamp1-EGFP, it was mainly present in the lumen. Therefore, LE/LYS appeared as red (CAV1-mCherry) spots with a green (EGFP-Rab7 and Lamp1-EGFP) boundary (Fig. 4 D). Because CAV1 is a membrane protein, it was most likely sequestered in the ILV that fill the lumen of LE/LYS. These results indicated that CAV1-mCherry did not only reach the early endosomal compartments but continued into the degradative branch of the endocytic pathway with accumulation in ILV of LE/LYS.

Cavin-1 associates with fully assembled caveolar scaffolds in the plasma membrane but not with biosynthetic intermediates or unassembled forms of CAV1 (Hill et al., 2008; Hayer et al., 2010). Therefore, we used cavin-1 as a sensor to assess the assembly state of CAV1 in the endosomal pathway. When coexpressed with EGFP-Rab5 and CAV1-HA, cavin-1–mCherry was found to colocalize with CAV1 in EE, indicating that early endosomal CAV1 is, at least partly, still assembled in caveolar scaffolds (Fig. 4 E). Conversely, when coexpressed with EGFP-Rab7 and CAV1-HA, cavin-1–mCherry did not colocalize with the late endosomal marker, most likely because CAV1 scaffolds had disassembled before reaching LE/LYS (Fig. 4 F). Disassembly of caveolar scaffolds may therefore be linked to progression of CAV1 in the endolysosomal pathway.

Visualization of CAV1 in LE/LYS in fixed cells was found to be problematic because of poor fixation of these organelles in CV1 cells with various different formaldehyde (FA)-based fixatives. This was most clearly observed when the process was followed in the microscope; the majority of Lamp1-EGFP–positive LE/LYS lost CAV1-mCherry after addition of FA (Fig. S2 B and Video 2). The lumenal CAV1-mCherry was released into the surrounding cytoplasm, leaving an empty Lamp1-EGFP labeled "ghost" behind. The limiting membranes of LE/LYS were apparently fixed properly, but the content of many vacuoles was lost. As a consequence, we avoided fixation when visualizing late compartments of the endocytic pathway and used live cell microscopy with fluorescently labeled proteins and cargo instead.

CAV1 in the acidic lumen of LE/LYS

CAV1 is embedded in the cytoplasmic leaflet of membranes with both N and C termini facing the cytosol. To be degraded, it must be exposed to the hydrolases in the lumen of LE/LYS. In analogy to degradation of cell surface receptors, this could occur by inclusion into inward budding vesicles during ILV formation followed by lysis or degradation of the ILV in LYS.

To test whether CAV1 was exposed to the acidic lumen of LE/LYS, we took advantage of the difference in pH sensitivity of mCherry and EGFP fluorescence. Although EGFP fluorescence is quenched at pH values <6 (pK_a 6.0), mCherry remains brightly fluorescent in acidic environments down to pH 4.5 (pK_a <4.5; Kneen et al., 1998; Shaner et al., 2004; Shaner et al., 2005). The pH ranges from 6.0 to 6.5 in EE and 5.5 in LE to 4.7 in LYS (Kielian and Cohn, 1982; Zen et al., 1992).

It has been shown that acidification of endosomes can be followed using protein cargo with a tandem tag that contains both EGFP and mCherry (Pankiv et al., 2007). EGFP fluorescence is quenched in LYS, whereas mCherry is not. Following a similar strategy, we coexpressed CAV1-mEGFP and CAV1-mCherry in CV1 cells and performed live cell confocal imaging. The caveolar spots in the plasma membrane and in the limiting membrane of endosomes were yellow, as expected of mixed fluorescence emitted by CAV1-mEGFP and -mCherry (Fig. 5 A, dashed inset). The diffuse staining of the plasma membrane representing free CAV1 was also yellow.

However, many cytoplasmic vacuoles had the bright red color of mCherry consistent with selective quenching of mEGFP (Pankiv et al., 2007). To test whether this was caused by low pH, cells expressing CAV1-mCherry were loaded with 100 nM LysoTracker green for 1 h and imaged live. Most if not all acidic organelles marked by LysoTracker were positive for CAV1-mCherry (Fig. 5 B). When cells coexpressing CAV1-mCherry and CAV1-mEGFP were treated with 0.2 µM BafA (12 h) to neutralize the lumenal pH, the vacuoles were all fluorescent both in mCherry and mEGFP channels (Fig. 5 C). Similar results were obtained when 20 mM NH_4Cl (12 h) was used instead of BafA (unpublished data).

Because the mEGFP and mCherry were tagged to the C terminus of CAV1, the topology dictated that they would be inside the ILV. The loss of green fluorescence must therefore have involved lysis of ILV and exposure of the interior of these vesicles to low pH. To follow this process in individual endosomes, cells coexpressing CAV1-mEGFP and CAV1-mCherry were imaged live for 45 min using an epifluorescence microscope. Numerous endosomes initially yellow were seen to lose their green mEGFP fluorescence over time, whereas the red mCherry fluorescence remained constant (Fig. 5 D–F; and Video 3). Importantly, the loss of mEGFP fluorescence was not caused by photobleaching, as the overall perinuclear mEGFP fluorescence remained constant (Fig. 5 D). The use of CAV1 constructs thus provided a method to follow the late stages in the maturation of individual endosomes and multivesicular bodies in living cells.

Together, our data argued for a model in which CAV1 present in endosomes was sequestered into ILV. As the endosomes matured and fused with LYS, it was exposed to the acidic lumen and eventually degraded. Overexpression of CAV1 and the lack of efficient caveolae assembly enhanced this process so that CAV1 became an easily detected component in the lumen of LE/LYS.

CAV1 is ubiquitinated, and ubiquitination is required for degradation

Targeting of membrane proteins to ILV is usually controlled by the addition of ubiquitin groups to their cytosolic domain (Raiborg and Stenmark, 2009). To determine whether CAV1 was ubiquitinated, HA-tagged CAV1 was expressed in HEK293 cells and immunoprecipitated from extracts using the anti-CAV1 (N20) antibody. Western blot analysis using anti-HA antibody revealed the presence of multiple slower migrating CAV1 species in addition to the major band of CAV1-HA (Fig. 6 A). Probing equivalent

Published November 1, 2010

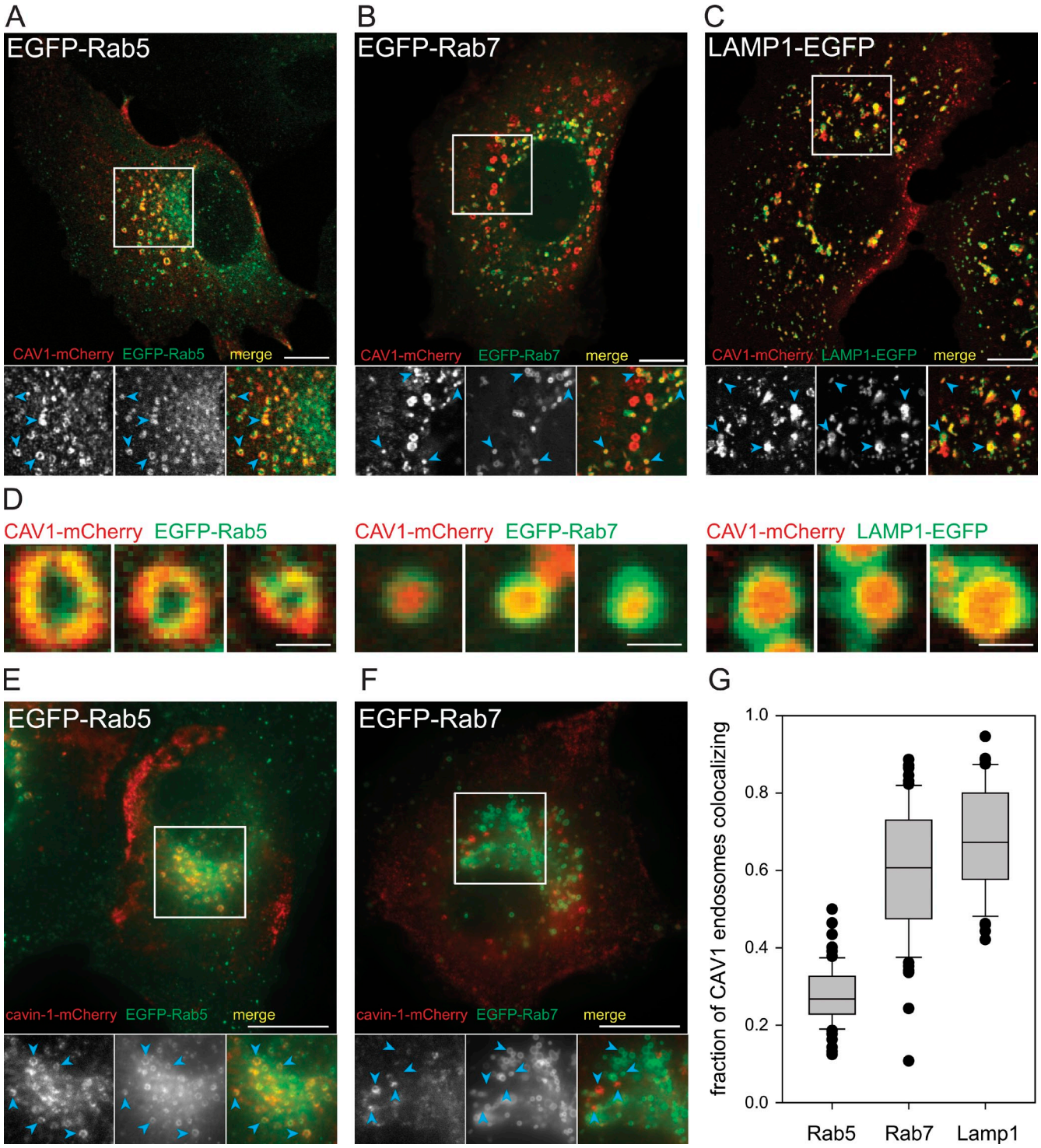

Figure 4. **CAV1 and cavin-1 in the endosomal pathway.** (A–C) CAV1-mCherry localized to Rab5-positive EE and to Rab7- and Lamp1-positive LE/LYS. Single confocal sections of fixed (A) or living (B and C) cells were acquired 12 h after transfection. (bottom) Insets show enlargements of boxed areas. (D) Enlarged views of individual organelles. In EE, CAV1-mCherry was present in the limiting membranes and, in LE/LYS, in the lumen of the organelles. (E and F) Cavin-1–mCherry localized to Rab5-positive EE but not to Rab7-positive LE. Cavin-1–mCherry was coexpressed with GFP-tagged endosomal makers and CAV1-HA (not depicted), and images acquired 12 h after transfection form living cells using an epifluorescence setup. (bottom) Insets show enlargements of the boxed areas. Arrowheads point to endosomal organelles indicating presence (A–C and E) or absence (F) of colocalization between markers. (G) Colocalization analysis of CAV1-mCherry endosomal structures with endosomal markers. The fraction of CAV1-mCherry endosomes per cell colocalizing with EGFP-Rab5 (n = 68 cells), EGFP-Rab7 (n = 68 cells), and Lamp1-EGFP (n = 43 cells) was determined as detailed in Materials and methods (Fig. S2 A) from images acquired from living cells using an epifluorescence setup. Box plots show medians, lower and upper quartiles (line and box), 10th and 90th percentiles (whiskers), and outliers (•). Bars: (A–C, E, and F) 10 µm; (D) 1 µm.

Published November 1, 2010

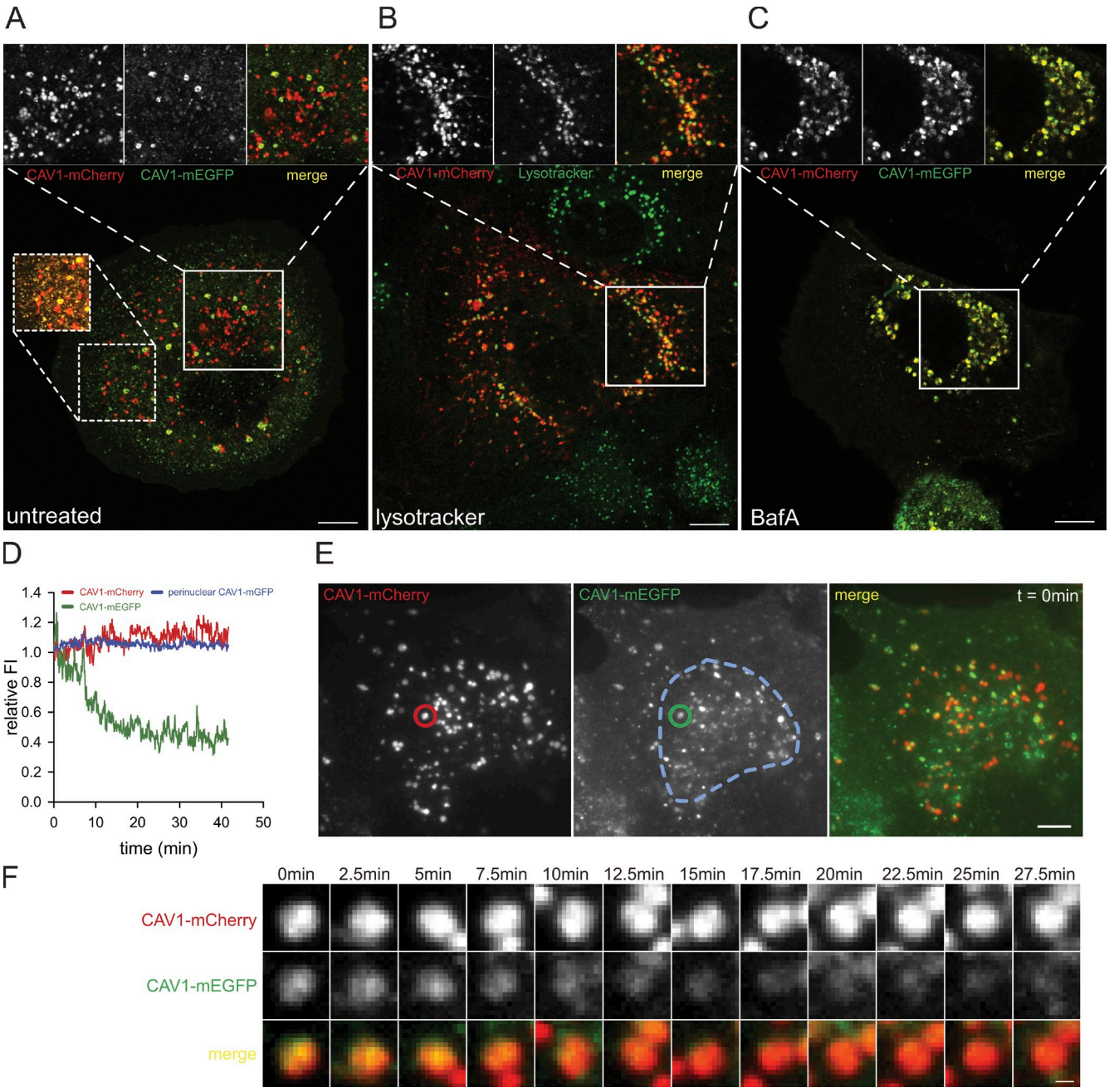

Figure 5. **CAV1 is exposed to the acidic lumen of LE/LYS.** (A) CAV1-mEGFP and CAV1-mCherry colocalized in caveolar spots in the plasma membrane (dashed inset, contrast adjusted) but not in many of the intracellular organelles when imaged live. (B) CV1 cells expressing CAV1-mCherry were stained with 100 nM LysoTracker (green) for 1 h and imaged live to identify acidic organelles. Most acidic organelles were positive for CAV1-mCherry. (C) Colocalization between CAV1-mEGFP and CAV1-mCherry in endosomes was restored by treatment of cells with 0.2 µM BafA (12 h), indicating acid quenching of mEGFP fluorescence. (A–C) Single confocal sections of live cells. (top) Insets show enlargements of boxed areas. (D and E) Live cell time-lapse imaging of CV1 cells coexpressing CAV1-mEGFP and CAV1-mCherry to monitor acid-dependent quenching of CAV1-mEGFP fluorescence during endosomal maturation. (D) An endosome initially positive for CAV1-mEGFP and CAV1-mCherry was tracked over 42 min as outlined in E, and fluorescence intensity profiles were plotted against time. CAV1-mEGFP fluorescence decayed over time, whereas CAV1-mCherry fluorescence was stable. To rule out photobleaching of mEGFP, the total perinuclear mEGFP fluorescence was measured and plotted (E, blue dashed outline; D, intensity profile). Time-lapse series were recorded with epifluorescence illumination at 0.2 Hz. (F) Stills of the CAV1-mEGFP and CAV1-mCherry–positive endosome tracked in D (Video 3). Bars: (A–C) 10 µm; (E) 5 µm; (F) 0.5 µm.

membranes with anti-ubiquitin (FK2) to detect ubiquitin revealed multiple corresponding bands (Fig. 6 A).

To confirm that CAV1 was the ubiquitinated species observed in the pull-down experiments, we engineered a version of CAV1 that could no longer be ubiquitinated as a result of mutation of all 12 lysines to arginines (CAV1-K*R; Fig. S3 A). When expressed in CV1 cells, a GFP-tagged form of the mutant readily reached the plasma membrane, where it was detectable as subresolution spots typical for caveolae (Fig. S3 B). Successful caveolae assembly of the mutant was also confirmed by sucrose velocity centrifugation of lysates prepared from cells expressing GFP- or HA-tagged CAV1-K*R (Fig. S3 C;

Published November 1, 2010

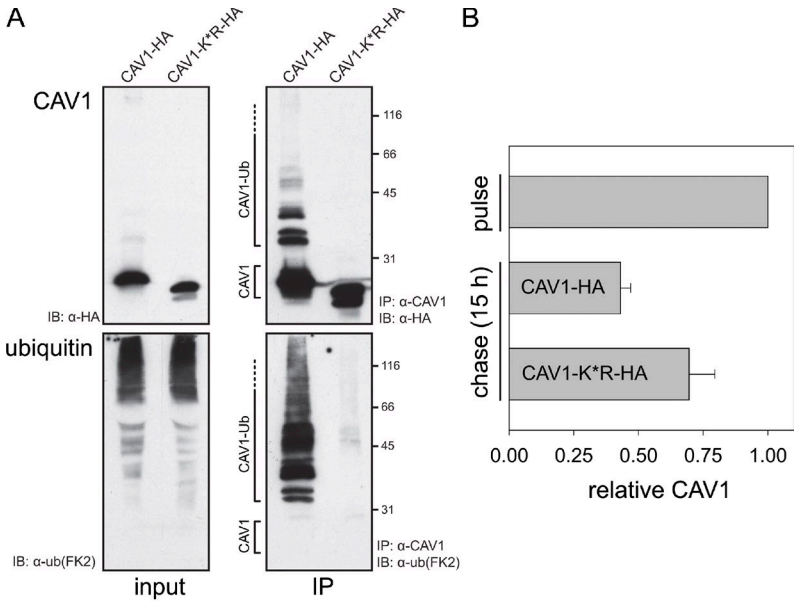

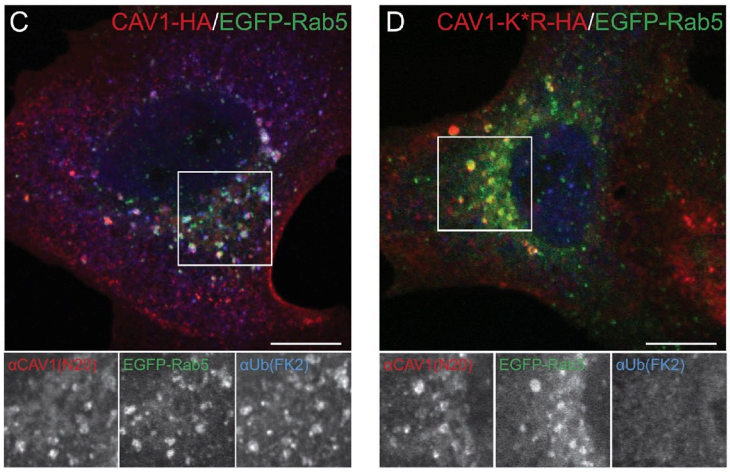

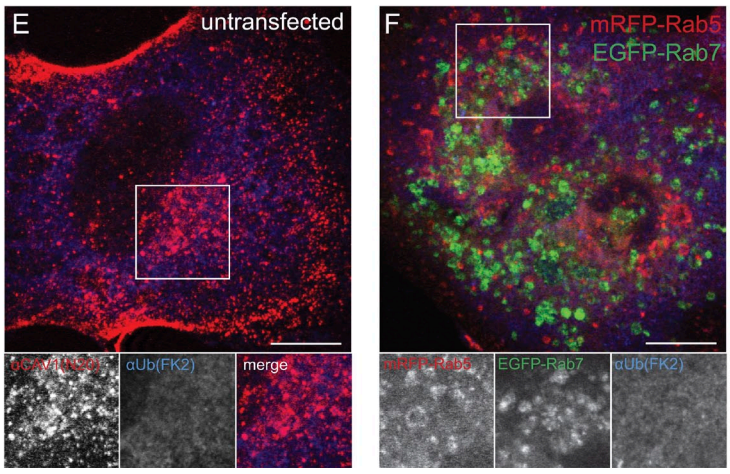

Figure 6. **CAV1 is ubiquitinated.** (A) HEK293 cells were transfected with CAV1-HA or CAV1-K*R-HA, and CAV1 was immunoprecipitated using anti-CAV1 (N20) antibody. Probing blots with anti-ubiquitin (FK2) antibody revealed ubiquitinated CAV1 species in immunoprecipitates prepared from cells expressing wild-type CAV1-HA but not from cells expressing the lysine-null mutant CAV1-K*R-HA. Migration of molecular mass standards is indicated in kilodaltons. (B) Pulse-chase analysis showed that turnover of CAV1-K*R-HA was slowed down by 47% when compared with wild-type CAV1 (CAV1-HA). Error bars indicate mean ± SD from three samples collected on two experimental days. (C) Ubiquitin staining accumulated and colocalized with overexpressed CAV1-HA in Rab5-positive EE of CV1 cells. (D–F) Accumulation of ubiquitin in EE was not observed in cells transfected with the lysine-null mutant CAV1-K*R-HA (D), in untransfected cells (E), or in cells transfected with mRFP-Rab5/EGFP-Rab7 (F). Single confocal sections of fixed cells are shown. (C–F, bottom) Insets show enlargements of boxed areas. Bars, 10 µm.

Hayer et al., 2010). When CAV1-K*R-HA was used in the pull-down experiment, no ubiquitinated species were observed, confirming that CAV1 was indeed ubiquitinated. CAV1 was also found to be ubiquitinated when immunoprecipitations were performed from lysates of HEK293 cells coexpressing CAV1-myc and HA-ubiquitin, both under native and denaturing conditions to exclude noncovalent association of ubiquitin conjugates (Fig. S3 D).

To determine whether the ubiquitinated CAV1 was present in EE, CV1 cells coexpressing CAV1-HA and EGFP-Rab5 were stained with both anti-CAV1 (N20) and anti-ubiquitin (FK2) antibodies. Confocal microscopy revealed extensive colocalization

Published November 1, 2010

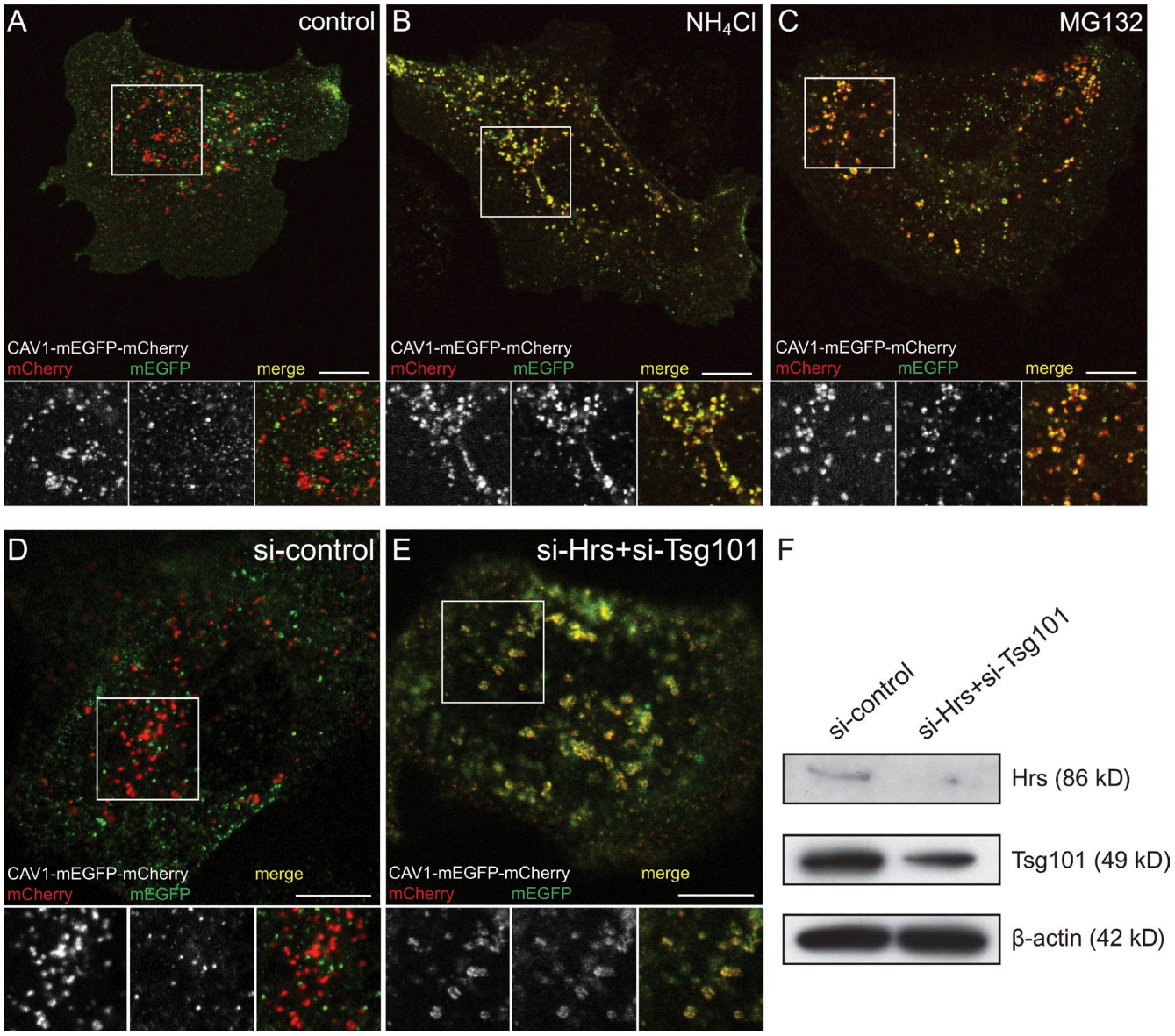

Figure 7. **CAV1 ubiquitination and ESCRT machinery are needed for ILV targeting.** (A) In CV1 cells expressing mEGFP-mCherry (tandem)–tagged CAV1, mCherry fluorescence did not overlap with mEGFP fluorescence in many endosomal structures, indicating acid-dependent quenching of mEGFP in LE/LYS (Fig. 5 A). (B and C) Treatment of cells with 20 mM NH_4Cl (B) or 10 µM MG132 (C) restored mEGFP fluorescence, which is consistent with neutralized lumenal pH and defects in ILV targeting, respectively. HeLa cells pretreated for 48 h with control siRNA (D) or siRNAs targeting ESCRT components Hrs and Tsg101 (E; double knockdown) were transfected with CAV1-tandem for 12 h and viewed live by confocal microscopy. The presence of yellow endosomes upon knockdown of Hrs and Tsg101 showed involvement of ESCRT machinery in ILV targeting of CAV1. (F) Western blot analysis indicated successful knockdown of Hrs and Tsg101. (A–E) Single confocal sections of live cells are shown. (bottom) Insets show enlargements of boxed areas. Bars, 10 µm.

between CAV1 and ubiquitin in Rab5-positive EE (Fig. 6 C). Strikingly, accumulation of anti-ubiquitin signal was observed only when cells were transfected with wild-type CAV1 but not with the lysine-null mutant CAV1-K*R (Fig. 6 D). Untransfected cells or cells transfected with tagged Rab5/Rab7 alone displayed a typical homogenous ubiquitin distribution in the cytoplasm and nucleus (Fig. 6, E and F). Therefore, ubiquitinated CAV1 was detectable only when abundant CAV1 was present in the endolysosomal pathway.

To directly address the relevance of ubiquitination for degradation of CAV1, we tested whether the lysine-null mutation affected the degradation kinetics of CAV1. Indeed, when CAV1-K*R-HA was tested in pulse-chase experiments, degradation of the mutant was reduced by 47% when compared with wild-type CAV1-HA, demonstrating that ubiquitination was important for CAV1 degradation (Fig. 6 B).

Together, the results showed that CAV1 was ubiquitinated. In cells overexpressing CAV1, the ubiquitinated forms accumulated in Rab5-positive EE. Ubiquitination was specifically required for CAV1 degradation because a mutant of CAV1 that could not be ubiquitinated displayed attenuated degradation kinetics.

Ubiquitination and ESCRT components Hrs and Tsg101 are required for ILV targeting of CAV1

If ubiquitination was required for ILV targeting of CAV1, depletion of free ubiquitin by treating cells with the proteasome

Published November 1, 2010

inhibitor MG132 was expected to prevent ILV targeting and exposure of CAV1 to the acidic lumen of endosomes. To address this possibility, we modified our dual-tagging strategy where CAV1-mCherry but not CAV1-mEGFP was visible in acidic LE/LYS by constructing CAV1 tagged with mEGFP and mCherry at its C terminus (tandem tag, CAV1-tandem). Although not affecting the subcellular localization of CAV1, the tandem tag provided higher fluorescence intensity and a more constant ratio of GFP/mCherry signal than coexpressing individually tagged CAV1. The presence of red endosomes was used as readout for successful targeting of CAV1-tandem to the acidic lumen of endosomes.

As expected, many endosomes were red in control cells, whereas endosomes were both red and green in cells treated with NH_4Cl (Fig. 7, A and B). Strikingly, in the presence of 10 µM MG132 (12 h), most endosomes remained both red and green, which is consistent with a ubiquitin- or proteasome-dependent inclusion of CAV1 in ILV during late endosomal maturation (Fig. 7 C) but also with the reduced rate of CAV1 degradation observed in the presence of MG132 (Fig. 3 B).

A similar strategy was followed to test the involvement of the ESCRT machinery in ILV targeting of CAV1. HeLa cells pretreated with siRNAs (48 h) targeting the ESCRT components Hrs and Tsg101 or control siRNA were transfected with CAV1-tandem, and endosomal CAV1 was visualized by confocal microscopy. Initial experiments, in which Hrs or Tsg101 were individually knocked down, did not produce a strong phenotype (unpublished data). However, upon double knockdown of both Hrs and Tsg101, severe defects in ILV targeting of CAV1-tandem were observed with CAV1-tandem–positive endosomes remaining both red and green (Fig. 7, D–F). Together, not only was CAV1 ubiquitinated and ubiquitination required for its degradation, but ubiquitin served as a sorting signal for ILV targeting of CAV1, a process that required ESCRT components Hrs and Tsg101.

Discussion

Caveolae in the plasma membrane are stable structures, and CAV1 is, correspondingly, a remarkably long-lived protein. However, when caveolae assembly was perturbed, we found that the fraction of unassembled CAV1 in cells was elevated, and the turnover dramatically accelerated. The protein was targeted to endosomes, ubiquitinated, sequestered into ILV by the ESCRT machinery, and degraded in LYS (Fig. 8). The results allowed us to explain observations regarding the life cycle of CAV1 and about the nature of caveolin-rich vacuoles called caveosomes, previously described after CAV1 overexpression by our group.

One of the perturbations used to increase the turnover of CAV1 was, indeed, its overexpression. Apparently, overabundance of this caveolar component resulted in saturation of caveolae assembly in the Golgi complex, generation of a rapidly diffusing pool of free CAV1 in the plasma membrane, and a drop in $t_{1/2}$ from >36 h for endogenous to 13.6 h for overexpressed CAV1. Silencing of cavin-1 resulted in a similar effect with an almost complete loss of 70S caveolar scaffolds in the cell, accumulation of 8S caveolin intermediates, and again, a diffuse plasma membrane distribution of CAV1. The reduction in cellular cholesterol using U18666A also dramatically increased the level of free, rapidly diffusing CAV1 in the plasma membrane at the expense of caveolae. Cholesterol is required for the assembly of caveolae in the Golgi; it binds directly to caveolins and serves as an essential component of the lipid raft–like membrane microdomain (Murata et al., 1995).

In addition to elevating the free CAV1 in the plasma membrane, these three conditions caused the accumulation of CAV1 in Lamp1-positive endolysosomal vacuoles in the cytoplasm. This indicated that excess, unassembled CAV1 was targeted to the degradative branch of the endocytic pathway. Inhibition with NH_4Cl and BafA confirmed that the degradation occurred in LYS.

Under normal, unperturbed conditions, CAV1 in the plasma membrane is localized in caveolae without a detectable free pool. It has been shown by immunofluorescence and with live cell imaging that some CAV1 also resides in EE, where it forms defined domains (Pol et al., 2000; Pelkmans et al., 2004). The binding of cavin-1 to early endosomal CAV1 indicated that CAV1 in the EE possessed, at least in part, the mature, assembled conformation.

That indirect immunofluorescence did not show a presence of endogenous CAV1 in LE or LYS may not only be because of its slow rate of turnover and its low abundance in these organelles but also because of a fixation artifact that makes it difficult to demonstrate antigens present in ILV of CV1 cells. Although EE were properly fixed using various FA-based fixatives, the majority of Lamp1-containing organelles ruptured during fixation and released their contents, including CAV1, into the cytoplasm. Therefore, to analyze late endosomal compartments, live cell imaging was more reliable than immunofluorescence microscopy but could only be performed with tagged forms of CAV1 and endosomal markers. In unperturbed, stable cell lines expressing fluorescently tagged CAV1 at relatively low levels, no staining was seen in LE/LYS. In contrast, transient overexpression of fluorescent CAV1 resulted in rapid accumulation in Rab5-, Rab7-, and Lamp1-positive organelles.

Electron microscopy using immunogold labeling in HepG2 cells has previously shown that endogenous CAV1 can be found in multivesicular bodies (Botos et al., 2008) and that stimulation of caveolar endocytosis with albumin increases targeting of CAV1 to this compartment, suggesting a correlation between caveolar trafficking and lysosomal CAV1 degradation. That degradation of endogenous CAV1 occurs in LYS is also supported by the observations that siRNA-mediated knockdown of flotillin-1 and cavin-1, as well as treatment of cells with PDGF, causes accelerated degradation of CAV1 and that this is sensitive to inhibitors of lysosomal degradation (Peterson et al., 2003; Hill et al., 2008; Vassilieva et al., 2009).

When CAV1 was overexpressed, a clear ubiquitin signal was observed in EE. Without CAV1 overexpression or after overexpression of the lysine-null mutant of CAV1, there was no such signal. Biochemical analysis confirmed that a large fraction of the CAV1 present in the cells was in fact poly- or monoubiquitinated and that ubiquitination was important for accelerated CAV1 degradation. Likewise, depletion of free ubiquitin by MG132 and siRNA knockdown of Hrs and Tsg101 showed that both ubiquitin and the ESCRT machinery were required to target CAV1 to ILV. Before closure of ILV, the cargo

Published November 1, 2010

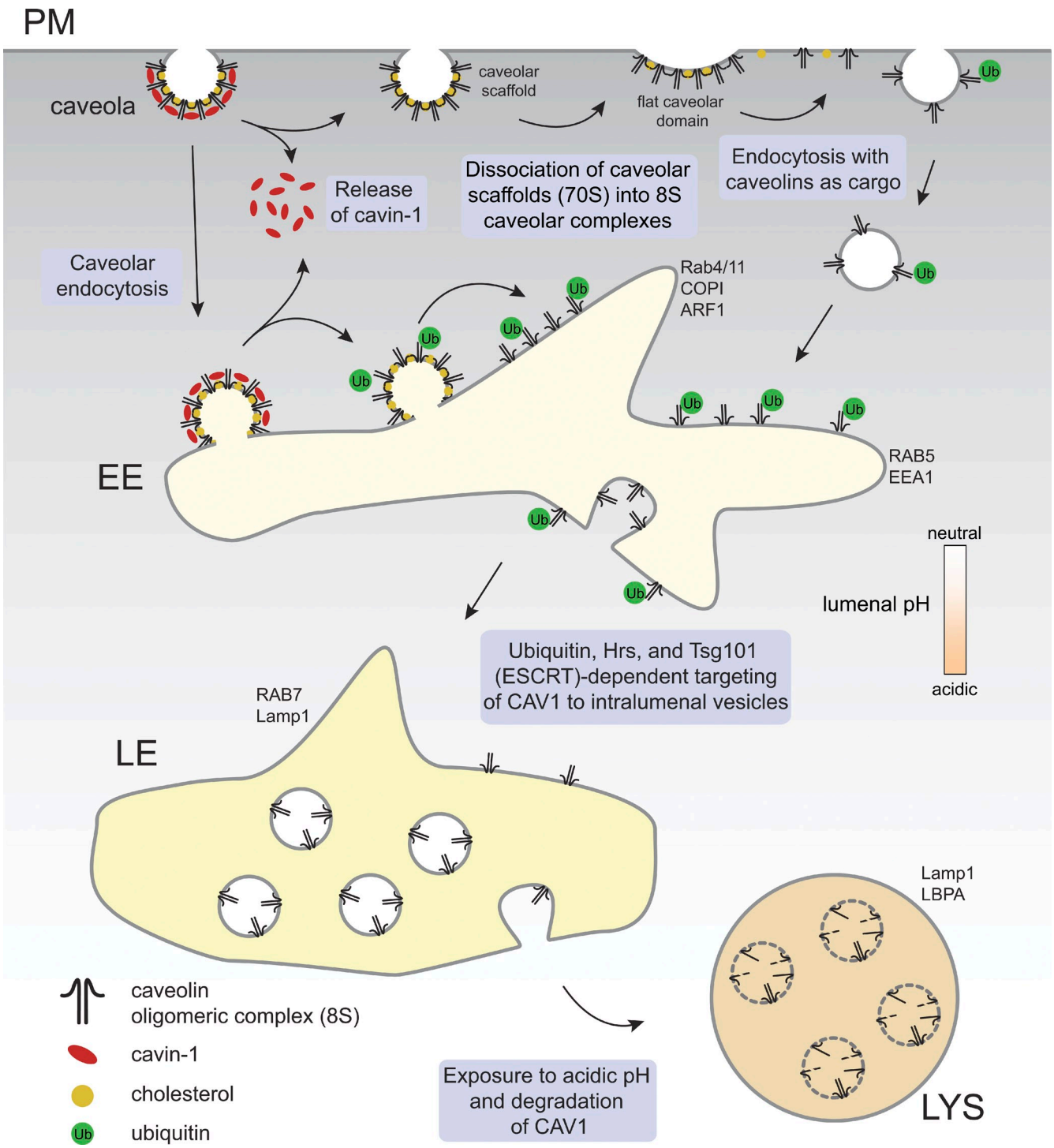

Figure 8. **Model of caveolae disassembly and degradation of CAV1.** Disassembly involves the release of cavin-1 from an intact caveola followed by dissociation of the destabilized 70S caveolar scaffold into 8S caveolar complexes. This may occur in EE after caveolar endocytosis or in the plasma membrane (PM), from where disassembled CAV1 is delivered to EE as endocytic cargo. Unassembled CAV1 may also arise when assembly of caveolar scaffolds in the Golgi is compromised and CAV1 arrives in the plasma membrane in the form of 8S complexes. In endosomes, the ubiquitinated 8S caveolar complexes are recognized by the ESCRT machinery and targeted to ILV facing the lumen. Upon lysis of ILV in LYS, CAV1 is exposed to the acidic vacuolar pH and degraded by proteolytic cleavage.

proteins to be degraded are usually deubiquitinated. The selective targeting of activated EGF receptor and other membrane proteins for destruction in LYS occurs in this way (Raiborg and Stenmark, 2009). When viewed in live cells, the CAV1 present in Rab7- and Lamp1-positive LE/LYS was in fact mainly localized in the lumen of the vacuoles and not in the limiting membrane, whereas in EE, its localization still coincided with Rab5 in the limiting membrane.

The quenching of CAV1-mEGFP fluorescence in LE/LYS observed in live cells showed that CAV1 in the ILV became

Published November 1, 2010

exposed to low pH. Given the membrane topology of CAV1 and the location of the GFP at the C terminus, this shift implied that the protection of the GFP by the ILV membrane was lost and the GFP exposed to a pH <6.0. After expressing CAV1 tagged with mEGFP and mCherry separately or in tandem, we could follow the maturation of individual endosomes in live cells by observing the shift from yellow to red fluorescence. Such a dual-tag strategy may be of general use in studies of ILV formation, acidification, and LE/LYS maturation in living cells.

Earlier experiments from our laboratory indicated that during entry into CAV1-EGFP–expressing CV1 cells, incoming SV40 in transit from the plasma membrane to the ER enters CAV1-rich intracellular organelles (Pelkmans et al., 2001). These organelles were called caveosomes because they seemed to differ from normal endosomes. They were characterized by the abundant presence of CAV1-EGFP, they did not contain endosomal markers, and their lumenal pH was neutral (Pelkmans et al., 2001).

Subsequently, we found that incoming viruses do in fact pass through EE and LE on their way to the ER, where penetration occurs (unpublished data). In view of the new SV40 data and the results presented in this study, we no longer consider caveosomes independent organelles. Under normal conditions, we find that endogenous CAV1 can be observed in EE but, typically, not in LE/LYS. However, when highly overexpressed, as it was in our studies describing caveosomes, CAV1-EGFP and other forms of CAV1 accumulated in late organelles of the endocytic pathway. These contain ILV and LE/LYS markers such as Rab7 and Lamp1. These are markers that were not tested in the original caveosome studies.

There may be several reasons why the original studies describing caveosomes (Pelkmans et al., 2001, 2004) came to the conclusion that their lumenal pH is neutral. The pH of CAV1-containing organelles was not determined directly, but inferred from bulk pH measurements using SV40 as a probe, from cells in suspension. Moreover, time course analysis of SV40 entry and drug wash-in experiments now suggest that the time point at which the pH was measured, using the fluorescent virus as the pH probe, was not well chosen because a large fraction of virus may have already reached the ER, i.e., a neutral environment, by the time the measurements were undertaken (unpublished data).

The electron micrographic sections showing structures with many caveolar domains most likely represent structures still connected to the plasma membrane (Parton and Simons, 2007; Kiss and Botos, 2009). We emphasize that caveosomes, according to our present data, are most likely modified LE/LYS and thus part of the classical endocytic pathway. We suggest that the term caveosome no longer be used.

In the light of our findings, we propose that the degradation of CAV1 occurs in LE/LYS after inclusion of CAV1 into ILV by the ESCRT complexes localized in EE (Fig. 8). Degradation only occurs if CAV1 is present in 8S complexes because the intact caveolar scaffolds are too big to be included in ILV. To be recognized by the ESCRT machinery and sequestered after deubiquitination in ILV, the 8S complexes must, moreover, be present in the EE and be ubiquitinated. The 8S complexes can be formed in the following different ways: (a) caveolar scaffolds in the plasma membrane may be destabilized, e.g., by the loss of cavin-1, followed by dissociation into 8S complexes and the endocytosis of these complexes into EE. (b) The assembly of caveolar scaffolds in the Golgi complex may be compromised, e.g., because of overexpression of CAV1 or lack of cholesterol, resulting in the arrival of unassembled, freely diffusing 8S complexes to the plasma membrane followed by endocytosis and delivery to EE. (c) In the absence of cavin-1, the caveolar scaffolds may still be assembled in the Golgi complex, but being unstable, they dissociate into 8S complexes soon after insertion into the plasma membrane (Hayer et al., 2010). (d) Dissociation of caveolar scaffolds may also occur in EE after endocytosis of intact caveolar domains in the form of caveolar vesicles and their fusion with EE. In this case, the loss of cavin-1 may allow dissociation of the endosomal caveolar scaffolds. The degradation of caveolae is a stepwise process involving many components. It remains to be determined how the disassembly of the highly stable, long-lived caveolar domain is regulated by ubiquitination, the cavins, and other cellular factors.

Materials and methods

Cell culture and transfections

CV1 and HeLa cells (American Type Culture Collection) were grown in DME (Invitrogen) supplemented with 10% FCS and 5% Glutamax (Invitrogen). HeLa cells stably expressing CAV1-mRFP (Tagawa et al., 2005) were maintained as HeLa cells but in the presence of 0.5 mg/ml G418. HEK293 cells were grown as CV1 but in the presence of penicillin/streptomycin. CV1 cells stably expressing CAV1-mEGFP (CV1-CAV1-mEGFP) were generated using the parental cell line CV1–Flp-In (Invitrogen) and the plasmid CAV1-mEGFP/FRT/TO, following the manufacturer's protocol for Flp-In recombination (Invitrogen). In a similar way, CV1-GFP-GPI cells were generated using the plasmid GFP-GPI/FRT/TO. Both recombinant cell lines were grown as CV1 cells but in the presence of 150 µg/ml hygromycin. CV1 cells were transfected with cDNA by electroporation according to the manufacturer's recommendation (Nucleofector kit V; program A24; Lonza), and HEK293 cells were transfected by the calcium phosphate method.

Plasmid constructs

CAV1-mEGFP, CAV1-mCherry, CAV1-HA, and cavin-1–mEGFP have been described previously (Hayer et al., 2010). To generate CAV1-mEGFP/FRT/TO, the coding sequence for CAV1-mEGFP was excised from the plasmid CAV1-mEGFP as HindIII–NotI fragment and ligated into appropriately digested pcDNA5/FRT/TO (Invitrogen). GFP-GPI/FRT/TO was generated by subcloning GFP-GPI from EGFP-GL-GPI (Keller et al., 2001) into pcDNA5/FRT/TO (Invitrogen) as HindIII–NotI fragment. CAV1-tandem was constructed first by PCR amplification of mEGFP flanked by BamHI and AgeI sites using primers (sense) 5′-ATGGATCCAGTGAGCAAGGGCGAGGAGC-3′ and (antisense) 5′-ATACCGGTTTGTACAGCTCGTCCATGCCG-3′ and ligation into BamHI–AgeI-digested CAV1-mCherry (pcDNA5/FRT/TO backbone), yielding CAV1-mEGFP-mCherry (CAV1-tandem). The cDNA encoding the CAV1 mutant with all 12 lysines mutated into arginines (CAV1-K*R) was synthesized by GENEART AG as a sequence flanked by HindIII–BamHI sites and a C-terminal HA tag followed by a NotI site. Ligation of the HindIII–NotI- or HindIII–BamHI-digested fragment into appropriately digested pmEGFP-N1 backbone fragments yielded CAV1-K*R-HA or CAV1-K*R-mEGFP, respectively. Cavin-1–mCherry was generated based on cavin-1–mEGFP by swapping mEGFP against mCherry as AgeI–BsrGI fragment. EGFP-Rab5 was provided by M. Zerial (Max Planck Institute of Molecular Cell Biology and Genetics, Dresden, Germany), EGFP-Rab7 and Lamp1-EGFP were provided by J. Gruenberg (University of Geneva, Geneva, Switzerland), HA-ubiquitin was provided by P. De Camilli (Yale University School of Medicine, New Haven, CT), and CAV1-myc was provided by J. Pessin (Albert Einstein College of Medicine, New York, NY). mRFP-Rab5 has been described previously (Vonderheit and Helenius, 2005). Plasmid constructs generated in this study will be made available through Addgene after publication.

Antibodies and other reagents

Rabbit pAb anti-CAV1 (N20; sc-894), mouse mAb anti-LAMP1 (sc-20011), and mouse mAb anti–c-myc (9E10; sc-40) were obtained from Santa Cruz Biotechnology, Inc., rabbit pAb anti-PTRF (polymerase I and transcript release factor; cavin-1) from Abcam (ab48824), rabbit pAb anti-giantin (PRB-114C) and mAb anti-HA from Covance (MMS-101P), mAb anti-Hrs

Published November 1, 2010

from Sigma-Aldrich (6D11; WH0009146M1), mAb anti-Tsg101 from Axxora (4A10; NB200-112), mouse mAb anti–β-actin from Sigma-Aldrich (AC-15; A1978), and mouse mAb anti-ubiquitin from Enzo Life Sciences, Inc. (FK2; BML-PW8810-0500). Rabbit pAb anti-calnexin was produced in house. Alexa Fluor–conjugated secondary antibodies for immunofluorescence and LysoTracker green were obtained from Invitrogen.

Velocity gradient centrifugation

Sucrose velocity gradient centrifugation was performed as described previously (Hayer et al., 2010). In brief, cells were solubilized at 25°C in 0.5% Triton X-100 (TX100) in TNE (20 mM Tris-HCl, pH 7.4, 100 mM NaCl, and 5 mM EDTA) supplemented with Complete protease inhibitor cocktail (Roche). Postnuclear supernatants were loaded onto 10–40% linear sucrose gradients prepared in 0.5% TX100/TNE and spun in a rotor (SW55Ti; Beckman Coulter) at 50,000 rpm (237,020 *g*) and 4°C for 255 min. Gradient fractions were analyzed by SDS-PAGE/Western blotting.

RNAi

The siRNA oligomers targeting PTRF/cavin-1 (SI04178496), Hrs (SI00288239), and Tsg101 (SI02655184) were purchased from QIAGEN and transfected into HeLa-CAV1-mRFP or HeLa cells at 10 nM using Lipofectamine RNAiMAX (Invitrogen) according to the manufacturer's recommendations and as previously described (Hayer et al., 2010). Nontargeting siRNA (AllStarsNeg; QIAGEN) was used as control siRNA. Cells were analyzed 60–72 h after transfection as indicated.

Metabolic labeling, immunoprecipitations, and autoradiography

Per sample, 3×10^5 cells expressing CAV1 variants for 6 h after electroporation or untransfected CV1 cells were first starved for 45 min in Cys/Met-free DME (Sigma-Aldrich) and pulse labeled for 1 h or 4 h, respectively, using 0.2 mCi/ml [^{35}S]Cys/Met Promix (NEG772007; PerkinElmer) in otherwise Cys/Met-deficient DMEM. Cells were washed with and chased in full medium (DMEM, 10% FCS, and 1% Glutamax) supplemented with 5 mM Cys, 5 mM Met, 50 mM Hepes, pH 7.4, and 1× penicillin/streptomycin. For drug treatments, CV1 cells expressing CAV1-HA were pulse labeled for 1 h and chased for 1 h before addition of drugs (10 mM leupeptin, 0.2 µM BafA in DMSO, 20 mM NH_4Cl, 5 µg/ml U18666A, and 10 µM MG132 in DMSO) to ensure that drugs did not interfere with delivery of labeled CAV1 to the plasma membrane. Cells chased for the indicated times (15 h total for drug treatments and CAV1-K*R-HA) were solubilized in 500 µl RIPA buffer (50 mM Tris-HCl, pH 7.4, 150 mM NaCl, 1 mM EDTA, 1% TX100, 1% Na-deoxycholate, and 0.1% SDS) supplemented with Complete protease inhibitor cocktail (Roche) at 4°C. For immunoprecipitations, lysates were incubated 2 h or overnight at 4°C with 2 µg anti-CAV1 (N20) antibody, and complexes were recovered with protein G–Sepharose (GE Healthcare). Immunoprecipitates were washed four times using RIPA buffer, eluted by boiling in SDS sample buffer, and separated by SDS-PAGE. Labeled protein was visualized using a phosphoimager (STORM; MDS Analytical Technologies), and bands were quantified with ImageJ (National Institutes of Health).

Native and denaturing immunoprecipitations for detection of ubiquitinated CAV1

HEK293 cells were transfected with CAV1-HA, CAV1-K*R-HA, empty vector, or cotransfected with CAV1-myc and HA-ubiquitin by the $Ca_3(PO_4)_2$ method. 24 h later, cells were scraped into PBS, pelleted, and solubilized in 250 µl immunoprecipitation buffer (150 mM KCl, 50 mM Tris, pH 7.4, 5 mM $MgCl_2$, 1% TX100, 5% glycerol, and 2 mM β-mercaptoethanol supplemented with Complete protease inhibitor cocktail). For denaturing immunoprecipitations, extracts prepared in 100 µl of immunoprecipitation buffer were first boiled in the presence of 1% SDS for 5 min and then diluted 1:10 using immunoprecipitation buffer containing 1 mg/ml BSA to yield 0.1% SDS final concentration. Lysates were spun down at 15,800 *g* for 10 min at 4°C, supernatants were incubated with 2 µg anti-CAV1 (N20) for 1.5 h at 4°C, and immunocomplexes were precipitated using protein G–Sepharose. 500 µg protein in 250 µl or 1 ml final volume was used for native or denaturing immunoprecipitates, respectively. Immunoprecipitates were resolved by SDS-PAGE and analyzed by Western blotting.

Immunofluorescence imaging

Cells grown on coverslips were fixed using 4% FA in PBS. Cells were permeabilized using 0.05% saponin and 1% BSA in PBS and incubated with the appropriate primary (1:500) and secondary (1:1,000) antibodies, and coverslips were mounted on slides using Immumount (Thermo Fisher Scientific). Imaging was performed on an inverted confocal microscope system (LSM 510 Meta; Carl Zeiss, Inc.) using a 100× 1.4 NA objective.

FRAP

For FRAP experiments, either CV1-CAV1-mEGFP cells untreated or treated with 5 µg/ml U18666A (16 h) or CV1-GFP-GPI cells were used. Coverslips with cells were transferred to a custom-built metal microscope coverslip chamber in CO_2-independent medium (Invitrogen) supplemented with 10% FCS. FRAP analyses were performed at 37°C on an inverted confocal microscope system (LSM 510 Meta) equipped with a temperature-controlled stage and a 63× 1.4 NA objective. A defined region of interest (4 × 4 µm) was bleached using the 488-nm line of a 30-mW Ar laser at high laser intensity (100% power, 100% transmission, and 30 iterations), and fluorescence recovery was recorded by scanning at low laser intensity (100% power and 10% transmission). Images were acquired as 12-bit LSM files at 512 × 512 pixels/frame and 0.14 µm/pixel lateral resolution. Image series with little or no apparent motion of cells were imported into ImageJ and automatically aligned using the TurboReg plug-in (http://bigwww.epfl.ch/thevenaz/turboreg/; Thévenaz et al., 1998). The mean fluorescence intensity of the region of interest was determined after background subtraction and normalization as described previously (Phair and Misteli, 2000).

Live cell fluorescence imaging

CV1 cells expressing fluorescently tagged constructs and seeded on 18-mm coverslips were transferred to a custom-built metal microscope coverslip chamber in CO_2-independent medium (Invitrogen) supplemented with 10% FCS. TIR and epifluorescence time-lapse imaging were performed on a microscope (IX71; Olympus) equipped with a camera (IMAGO QE; TILL Photonics), dual condenser (TIR/EPI; TILL Photonics), ArKr laser (Spectra Physics), acousto-optic tunable filters (Optoelectronics, Inc.), a monochromatic light source polychrome IV (TILL Photonics), a dual-view beam splitter (Optical Insights) in the emission light path, a 60× 1.45 NA objective, and a temperature-controlled incubation chamber, and using MetaMorph software (MDS Analytical Technologies). For TIR illumination of CAV1-mEGFP, the 488-nm laser line was used, and the depth of the evanescent field was adjusted such that both ventral cell surface and parts of the Golgi complex were illuminated. For epiillumination, the monochromator was used at 488 and 568 nm with a beam splitter in the detection light path to avoid cross talk between mEGFP and mCherry signals. Confocal live cell imaging was performed on a system (LSM 510 Meta) equipped with a 100× 1.4 NA objective and a temperature-controlled stage.

Colocalization analysis

Images were acquired from living cells expressing CAV1-mCherry and EGFP-tagged endosomal markers using the aforementioned system (IX71; Olympus) using a monochromatic light source (EPI illumination), a 60× 1.45 NA objective, and a filter wheel in the emission light path. A custom-written analysis routine implemented in MATLAB (MathWorks) was used to detect endosomal structures and determine overlap (Gupta et al., 2009). About 6×10^4 endosomes were analyzed in total from $n = 68$ cells for CAV1-mCherry/Rab5-EGFP, $n = 68$ cells for CAV1-mCherry/Rab7-EGFP, and $n = 43$ cells for CAV1-mCherry/Lamp1-EGFP.

Online supplemental material

Fig. S1 shows expression levels of CAV1-mRFP and CAV1-mEGFP stably transfected in HeLa and CV1 cells, respectively, relative to endogenous CAV1. Both fusion proteins were efficiently incorporated into 8S/70S-equivalent caveolar complexes. Fig. S1 also shows that accumulation of CAV1 in endosomal organelles upon overexpression could not be reversed by co-overexpression of cavin-1. Fig. S2 illustrates the automated colocalization analysis method used and shows how CAV1-mCherry in the lumen of LE/LYS but not the LE/LYS membrane marker Lamp1-EGFP was lost during FA fixation. Fig. S3 describes and characterizes the lysine-null mutant of CAV1 (CAV1-K*R) by showing that the mutant was efficiently incorporated into 8S/70S-equivalent caveolar complexes when expressed in CV1 cells and that it reached the plasma membrane, where it localized to caveolar spots. Fig. S3 also shows immunoprecipitations of CAV1 performed under denaturing conditions, confirming that CAV1 is ubiquitinated. Video 1 shows that, in cells pretreated with U18666A, newly synthesized CAV1-mEGFP reached the plasma membrane in unassembled form. Video 2 illustrates that in LE/LYS, lumenal CAV1-mCherry was lost short after addition of FA fixative, whereas Lamp1-EGFP in the limiting membranes was properly fixed. In Video 3, our dual-tag strategy was used to follow targeting of CAV1-tandem to the acidic lumen of individual maturing endosomes. Online supplemental material is available at http://www.jcb.org/cgi/content/full/jcb.201003086/DC1.

We thank Gautam Dey for providing colocalization analysis scripts and Pietro De Camilli, Jean Gruenberg, Jeffrey Pessin, Kai Simons, and Marino Zerial for generous gifts of plasmids. We are grateful to Fabian Herzog for preparing the cell line CV1-GFP-GPI. We also thank Jason Mercer for comments on the manuscript and the Helenius laboratory for support and helpful advice.

Funding was provided by a DOC graduate fellowship (Doktorandenprogramm der Österreichischen Akademie der Wissenschaften) to A. Hayer from the Austrian Academy of Sciences, by a graduate fellowship from Boehringer Ingelheim Fonds to M. Stoeber, by ETH Zurich, and by the Swiss National Science Foundation.

Submitted: 19 March 2010
Accepted: 28 September 2010

References

Bastiani, M., L. Liu, M.M. Hill, M.P. Jedrychowski, S.J. Nixon, H.P. Lo, D. Abankwa, R. Luetterforst, M. Fernandez-Rojo, M.R. Breen, et al. 2009. MURC/Cavin-4 and cavin family members form tissue-specific caveolar complexes. *J. Cell Biol.* 185:1259–1273. doi:10.1083/jcb.200903053

Botos, E., J. Klumperman, V. Oorschot, B. Igyártó, A. Magyar, M. Oláh, and A.L. Kiss. 2008. Caveolin-1 is transported to multi-vesicular bodies after albumin-induced endocytosis of caveolae in HepG2 cells. *J. Cell. Mol. Med.* 12(5A):1632–1639. doi:10.1111/j.1582-4934.2007.00167.x

Cubells, L., S. Vilà de Muga, F. Tebar, P. Wood, R. Evans, M. Ingelmo-Torres, M. Calvo, K. Gaus, A. Pol, T. Grewal, and C. Enrich. 2007. Annexin A6-induced alterations in cholesterol transport and caveolin export from the Golgi complex. *Traffic.* 8:1568–1589. doi:10.1111/j.1600-0854.2007.00640.x

Dupree, P., R.G. Parton, G. Raposo, T.V. Kurzchalia, and K. Simons. 1993. Caveolae and sorting in the trans-Golgi network of epithelial cells. *EMBO J.* 12:1597–1605.

Fernandez, I., Y. Ying, J. Albanesi, and R.G. Anderson. 2002. Mechanism of caveolin filament assembly. *Proc. Natl. Acad. Sci. USA.* 99:11193–11198. doi:10.1073/pnas.172196599

Galbiati, F., D. Volonte, C. Minetti, D.B. Bregman, and M.P. Lisanti. 2000. Limb-girdle muscular dystrophy (LGMD-1C) mutants of caveolin-3 undergo ubiquitination and proteasomal degradation. Treatment with proteasomal inhibitors blocks the dominant negative effect of LGMD-1C mutanta and rescues wild-type caveolin-3. *J. Biol. Chem.* 275:37702–37711. doi:10.1074/jbc.M006657200

Gupta, G.D., M.G. Swetha, S. Kumari, R. Lakshminarayan, G. Dey, and S. Mayor. 2009. Analysis of endocytic pathways in *Drosophila* cells reveals a conserved role for GBF1 in internalization via GEECs. *PLoS One.* 4:e6768. doi:10.1371/journal.pone.0006768

Hansen, C.G., N.A. Bright, G. Howard, and B.J. Nichols. 2009. SDPR induces membrane curvature and functions in the formation of caveolae. *Nat. Cell Biol.* 11:807–814. doi:10.1038/ncb1887

Hayer, A., M. Stoeber, C. Bissig, and A. Helenius. 2010. Biogenesis of caveolae: stepwise assembly of large caveolin and cavin complexes. *Traffic.* 11:361–382. doi:10.1111/j.1600-0854.2009.01023.x

Hill, M.M., M. Bastiani, R. Luetterforst, M. Kirkham, A. Kirkham, S.J. Nixon, P. Walser, D. Abankwa, V.M. Oorschot, S. Martin, et al. 2008. PTRF-cavin, a conserved cytoplasmic protein required for caveola formation and function. *Cell.* 132:113–124. doi:10.1016/j.cell.2007.11.042

Keller, P., D. Toomre, E. Díaz, J. White, and K. Simons. 2001. Multicolour imaging of post-Golgi sorting and trafficking in live cells. *Nat. Cell Biol.* 3:140–149. doi:10.1038/35055042

Kielian, M.C., and Z.A. Cohn. 1982. Intralysosomal accumulation of polyanions. II. Polyanion internalization and its influence on lysosomal pH and membrane fluidity. *J. Cell Biol.* 93:875–882. doi:10.1083/jcb.93.3.875

Kirkham, M., A. Fujita, R. Chadda, S.J. Nixon, T.V. Kurzchalia, D.K. Sharma, R.E. Pagano, J.F. Hancock, S. Mayor, and R.G. Parton. 2005. Ultrastructural identification of uncoated caveolin-independent early endocytic vehicles. *J. Cell Biol.* 168:465–476. doi:10.1083/jcb.200407078

Kiss, A.L., and E. Botos. 2009. Ocadaic acid retains caveolae in multicaveolar clusters. *Pathol. Oncol. Res.* 15:479–486. doi:10.1007/s12253-008-9139-4

Kneen, M., J. Farinas, Y. Li, and A.S. Verkman. 1998. Green fluorescent protein as a noninvasive intracellular pH indicator. *Biophys. J.* 74:1591–1599. doi:10.1016/S0006-3495(98)77870-1

Liu, L., and P.F. Pilch. 2008. A critical role of cavin (polymerase I and transcript release factor) in caveolae formation and organization. *J. Biol. Chem.* 283:4314–4322. doi:10.1074/jbc.M707890200

Longva, K.E., F.D. Blystad, E. Stang, A.M. Larsen, L.E. Johannessen, and I.H. Madshus. 2002. Ubiquitination and proteasomal activity is required for transport of the EGF receptor to inner membranes of multivesicular bodies. *J. Cell Biol.* 156:843–854. doi:10.1083/jcb.200106056

McMahon, K.A., H. Zajicek, W.P. Li, M.J. Peyton, J.D. Minna, V.J. Hernandez, K. Luby-Phelps, and R.G. Anderson. 2009. SRBC/cavin-3 is a caveolin adapter protein that regulates caveolae function. *EMBO J.* 28:1001–1015. doi:10.1038/emboj.2009.46

Monier, S., R.G. Parton, F. Vogel, J. Behlke, A. Henske, and T.V. Kurzchalia. 1995. VIP21-caveolin, a membrane protein constituent of the caveolar coat, oligomerizes in vivo and in vitro. *Mol. Biol. Cell.* 6:911–927.

Murata, M., J. Peränen, R. Schreiner, F. Wieland, T.V. Kurzchalia, and K. Simons. 1995. VIP21/caveolin is a cholesterol-binding protein. *Proc. Natl. Acad. Sci. USA.* 92:10339–10343. doi:10.1073/pnas.92.22.10339

Pankiv, S., T.H. Clausen, T. Lamark, A. Brech, J.A. Bruun, H. Outzen, A. Øvervatn, G. Bjørkøy, and T. Johansen. 2007. p62/SQSTM1 binds directly to Atg8/LC3 to facilitate degradation of ubiquitinated protein aggregates by autophagy. *J. Biol. Chem.* 282:24131–24145. doi:10.1074/jbc.M702824200

Parat, M.O. 2009. The biology of caveolae: achievements and perspectives. *Int. Rev. Cell Mol. Biol.* 273:117–162. doi:10.1016/S1937-6448(08)01804-2

Parton, R.G., and K. Simons. 2007. The multiple faces of caveolae. *Nat. Rev. Mol. Cell Biol.* 8:185–194. doi:10.1038/nrm2122

Pelkmans, L., and M. Zerial. 2005. Kinase-regulated quantal assemblies and kiss-and-run recycling of caveolae. *Nature.* 436:128–133. doi:10.1038/nature03866

Pelkmans, L., J. Kartenbeck, and A. Helenius. 2001. Caveolar endocytosis of simian virus 40 reveals a new two-step vesicular-transport pathway to the ER. *Nat. Cell Biol.* 3:473–483. doi:10.1038/35074539

Pelkmans, L., T. Bürli, M. Zerial, and A. Helenius. 2004. Caveolin-stabilized membrane domains as multifunctional transport and sorting devices in endocytic membrane traffic. *Cell.* 118:767–780. doi:10.1016/j.cell.2004.09.003

Peterson, T.E., M.E. Guicciardi, R. Gulati, L.S. Kleppe, C.S. Mueske, M. Mookadam, G. Sowa, G.J. Gores, W.C. Sessa, and R.D. Simari. 2003. Caveolin-1 can regulate vascular smooth muscle cell fate by switching platelet-derived growth factor signaling from a proliferative to an apoptotic pathway. *Arterioscler. Thromb. Vasc. Biol.* 23:1521–1527. doi:10.1161/01.ATV.0000081743.35125.05

Phair, R.D., and T. Misteli. 2000. High mobility of proteins in the mammalian cell nucleus. *Nature.* 404:604–609. doi:10.1038/35007077

Pol, A., A. Lu, M. Pons, S. Peiró, and C. Enrich. 2000. Epidermal growth factor-mediated caveolin recruitment to early endosomes and MAPK activation. Role of cholesterol and actin cytoskeleton. *J. Biol. Chem.* 275:30566–30572. doi:10.1074/jbc.M001131200

Raiborg, C., and H. Stenmark. 2009. The ESCRT machinery in endosomal sorting of ubiquitylated membrane proteins. *Nature.* 458:445–452. doi:10.1038/nature07961

Razani, B., J.A. Engelman, X.B. Wang, W. Schubert, X.L. Zhang, C.B. Marks, F. Macaluso, R.G. Russell, M. Li, R.G. Pestell, et al. 2001. Caveolin-1 null mice are viable but show evidence of hyperproliferative and vascular abnormalities. *J. Biol. Chem.* 276:38121–38138. doi:10.1074/jbc/M1050408200

Razani, B., S.E. Woodman, and M.P. Lisanti. 2002. Caveolae: from cell biology to animal physiology. *Pharmacol. Rev.* 54:431–467. doi:10.1124/pr.54.3.431

Rothberg, K.G., J.E. Heuser, W.C. Donzell, Y.S. Ying, J.R. Glenney, and R.G. Anderson. 1992. Caveolin, a protein component of caveolae membrane coats. *Cell.* 68:673–682. doi:10.1016/0092-8674(92)90143-Z

Scheiffele, P., P. Verkade, A.M. Fra, H. Virta, K. Simons, and E. Ikonen. 1998. Caveolin-1 and -2 in the exocytic pathway of MDCK cells. *J. Cell Biol.* 140:795–806. doi:10.1083/jcb.140.4.795

Shaner, N.C., R.E. Campbell, P.A. Steinbach, B.N. Giepmans, A.E. Palmer, and R.Y. Tsien. 2004. Improved monomeric red, orange and yellow fluorescent proteins derived from Discosoma sp. red fluorescent protein. *Nat. Biotechnol.* 22:1567–1572. doi:10.1038/nbt1037

Shaner, N.C., P.A. Steinbach, and R.Y. Tsien. 2005. A guide to choosing fluorescent proteins. *Nat. Methods.* 2:905–909. doi:10.1038/nmeth819

Tagawa, A., A. Mezzacasa, A. Hayer, A. Longatti, L. Pelkmans, and A. Helenius. 2005. Assembly and trafficking of caveolar domains in the cell: caveolae as stable, cargo-triggered, vesicular transporters. *J. Cell Biol.* 170:769–779. doi:10.1083/jcb.200506103

Thévenaz, P., U.E. Ruttimann, and M. Unser. 1998. A pyramid approach to subpixel registration based on intensity. *IEEE Trans. Image Process.* 7:27–41. doi:10.1109/83.650848

Thomsen, P., K. Roepstorff, M. Stahlhut, and B. van Deurs. 2002. Caveolae are highly immobile plasma membrane microdomains, which are not involved in constitutive endocytic trafficking. *Mol. Biol. Cell.* 13:238–250. doi:10.1091/mbc.01-06-0317

Toomre, D., P. Keller, J. White, J.C. Olivo, and K. Simons. 1999. Dual-color visualization of trans-Golgi network to plasma membrane traffic along microtubules in living cells. *J. Cell Sci.* 112:21–33.

Vassilieva, E.V., A.I. Ivanov, and A. Nusrat. 2009. Flotillin-1 stabilizes caveolin-1 in intestinal epithelial cells. *Biochem. Biophys. Res. Commun.* 379:460–465. doi:10.1016/j.bbrc.2008.12.118

Vonderheit, A., and A. Helenius. 2005. Rab7 associates with early endosomes to mediate sorting and transport of Semliki forest virus to late endosomes. *PLoS Biol.* 3:e233. doi:10.1371/journal.pbio.0030233

Zen, K., J. Biwersi, N. Periasamy, and A.S. Verkman. 1992. Second messengers regulate endosomal acidification in Swiss 3T3 fibroblasts. *J. Cell Biol.* 119:99–110. doi:10.1083/jcb.119.1.99

Published November 1, 2010

Hayer et al., http://www.jcb.org/cgi/content/full/jcb.201003086/DC1

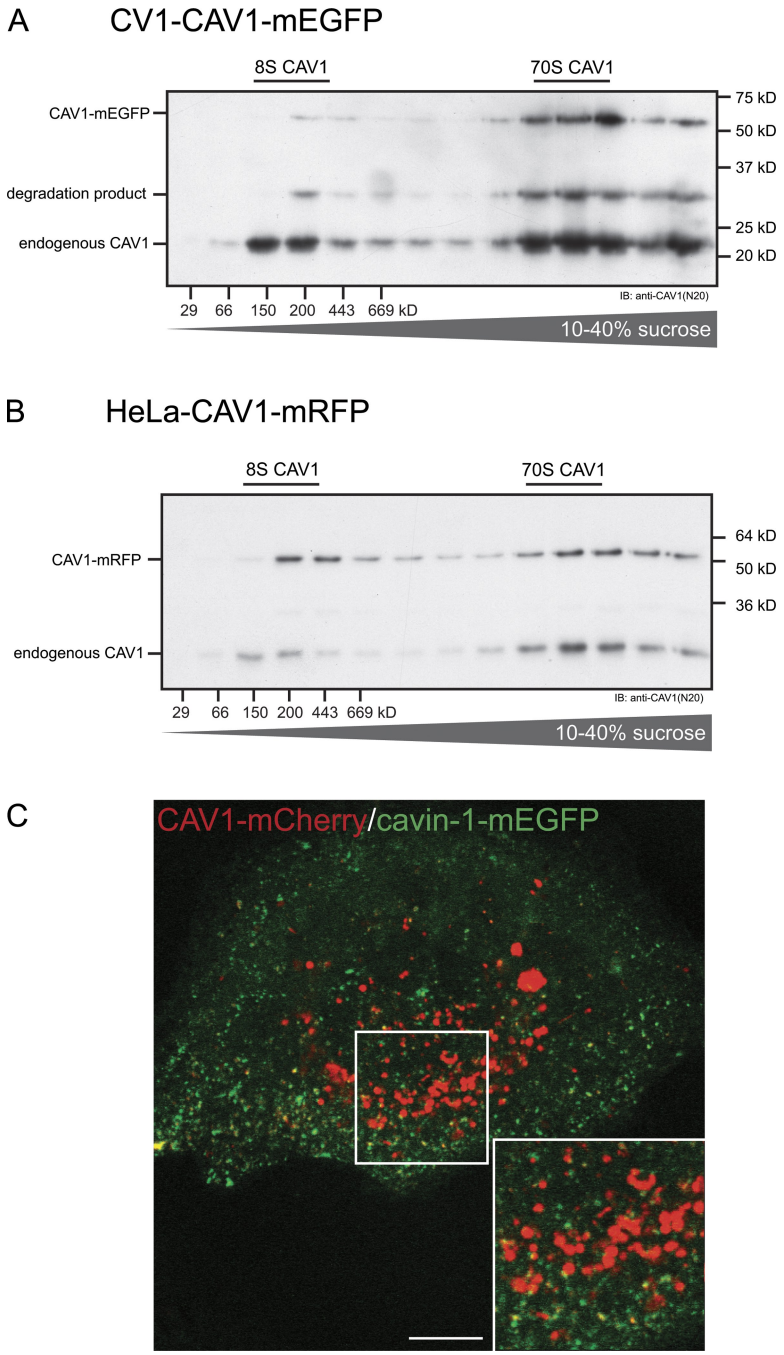

Figure S1. **Expression levels of cell lines stably transfected with fluorescent CAV1 constructs.** (A and B) CV1 cells stably expressing CAV1-mEGFP (A) or HeLa cells stably expressing CAV1-mRFP (B) were lysed, run through sucrose velocity gradients, fractions resolved by SDS-PAGE/Western blotting, and CAV1 detected using anti-CAV1 (N20) antibody. Both CAV1-mEGFP and CAV1-mRFP were efficiently incorporated into 8S/70S-equivalent caveolar complexes and expressed at similar levels as endogenous CAV1, resulting in moderate overexpression. (B) A full scan of the same blot shown in Fig. 2 A (si-control). (C) Co-overexpression of cavin-1 with CAV1 did not reverse targeting of CAV1 to intracellular vacuoles. CAV1-mCherry and cavin-1–mEGFP were cotransfected into CV1 cells and imaged live 12 h after transfection. A single confocal section is shown. Inset shows an enlargement of the boxed area. Bar, 10 µm.

Published November 1, 2010

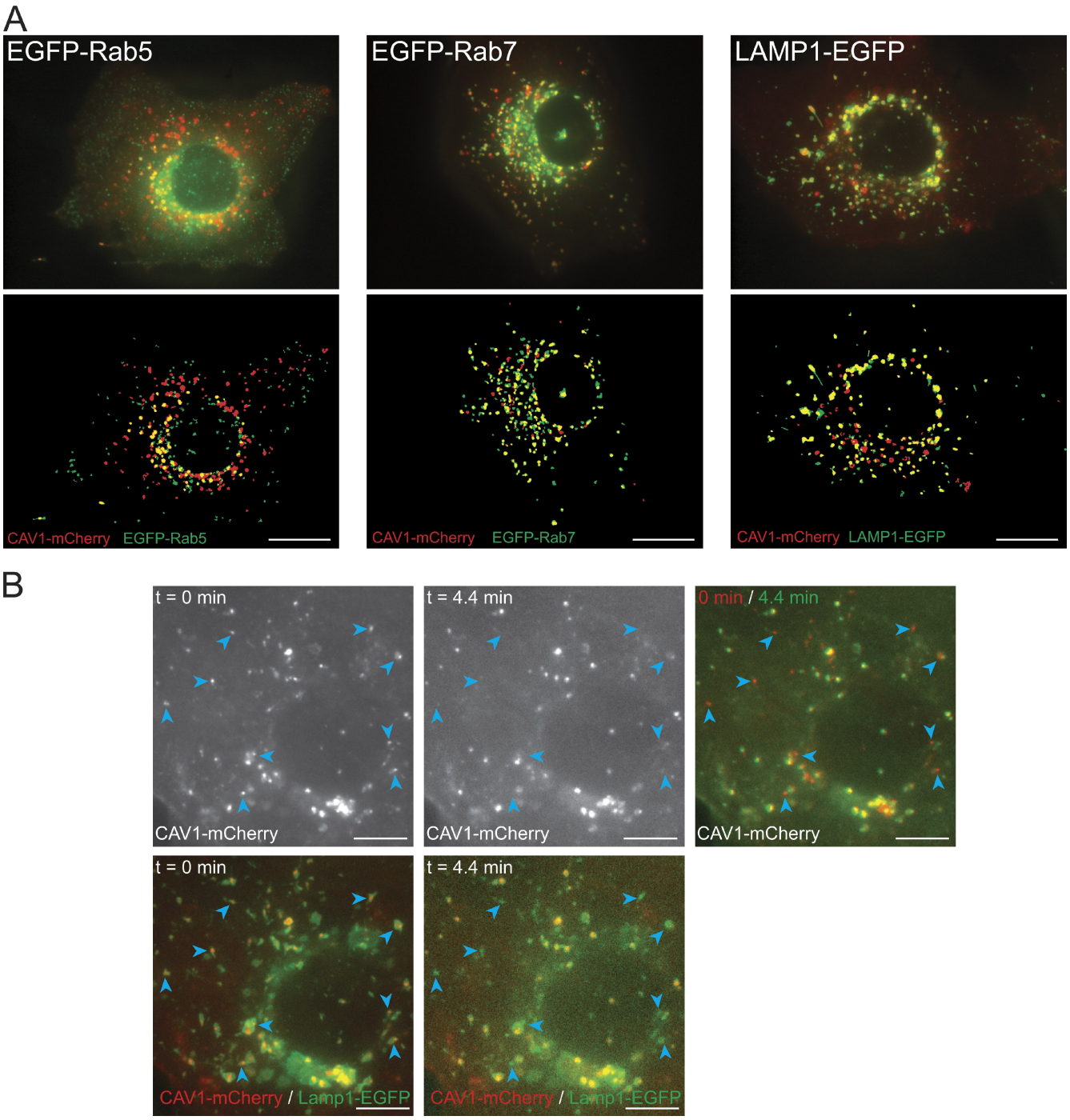

Figure S2. **Colocalization analysis and loss of late endosomal CAV1 during fixation.** (A) For quantitative colocalization analysis, CV1 cells cotransfected with CAV1-mCherry and either EGFP-Rab5, EGFP-Rab7, or Lamp1-EGFP were imaged live using an epifluorescence microscope. Examples of original images (contrast enhanced) and corresponding automatically detected endosomes are shown. (B) A time-lapse series of a CV1 cell coexpressing Lamp1-EGFP and CAV1-mCherry was acquired during and after FA fixative addition. t = 0 min marks the time when FA was added. Note the disappearance of the lumenal content (CAV1-mCherry) of LE/LYS short after addition of FA (arrowheads), whereas the limiting membrane (Lamp1-EGFP) remained intact (Video 2). Bars, 10 µm.

Published November 1, 2010

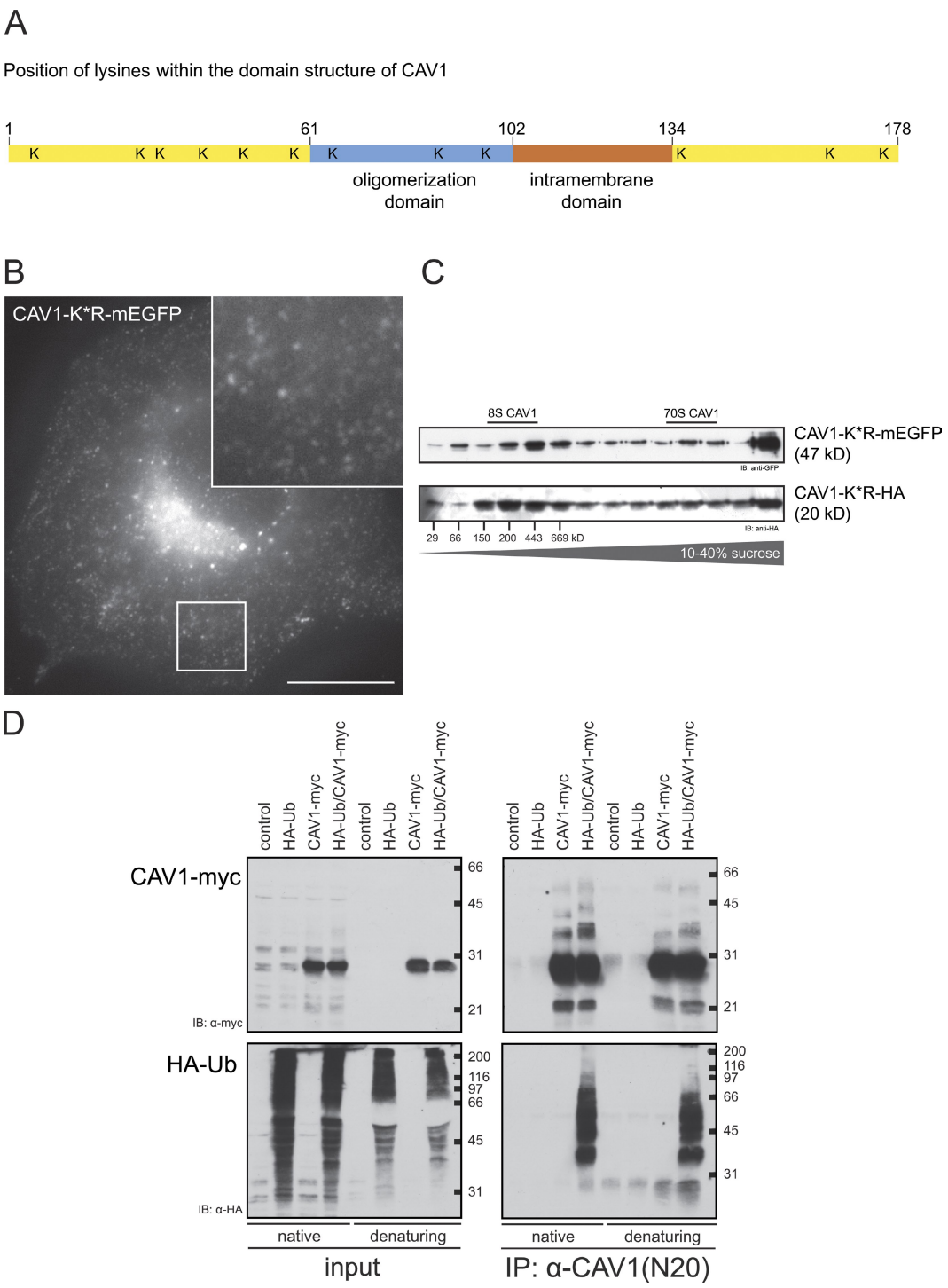

Figure S3. **The lysine-null mutant CAV1-K*R and denaturing immunoprecipitations to detect ubiquitinated CAV1.** (A) To generate CAV1-K*R constructs, all 12 lysines in CAV1 were mutated to arginines. (B) CV1 cells transfected with CAV1-K*R-mEGFP displayed normal cellular distribution of expressed mutant protein in the Golgi, in caveolar spots at the cell surface, and associated with endosomal structures. Inset shows an enlargement of boxed area. (C) When expressed in CV1 cells, both CAV1-K*R-mEGFP and CAV1-K*R-HA assembled into 8S- and 70S-equivalent caveolar complexes, indicating successful caveolae assembly. (D) HEK293 cells were transfected with HA-ubiquitin (HA-Ub), CAV1-myc, or cotransfected with both constructs (left). CAV1 was immunoprecipitated using anti-CAV1 (N20) antibody either under native or denaturing conditions (see Materials and methods). Probing blots with anti-HA antibody revealed ubiquitinated CAV1 species in immunoprecipitates prepared from cells overexpressing CAV1-myc. Migration of molecular mass standards is indicated in kilodaltons. Bar, 10 µm.

Published November 1, 2010

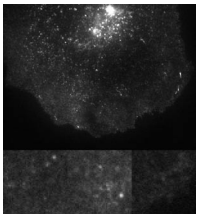

Video 1. **Surface delivery of CAV1-mEGFP in U18666A-treated cells.** CV1 cells treated with 5 µM U18666A (16 h) were transfected with CAV1-mEGFP using electroporation (see Materials and methods) and incubated in the presence of 1 mM cycloheximide during cell attachment (2 h). Expression of CAV1-mEGFP was induced by washout of cycloheximide, and cells were imaged by TIR-FM 60 min after washout. The evanescent field was adjusted such that both cell surface and part of the Golgi were visible. CAV1-mEGFP can be observed in tubular post-Golgi carriers. Upon arrival at the cell surface, they release their cargo, visible as burst of fluorescence diffusing laterally into the plasma membrane. Boxed areas showing examples are enlarged below. Time-lapse sequences were acquired at 1 Hz with an integration time of 500 ms/frame. Video is displayed at 15× real time.

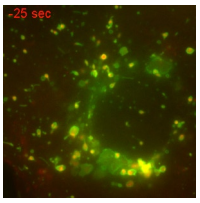

Video 2. **The limiting membranes but not the lumenal contents of LE/LYS can be fixed by FA.** CV1 cells coexpressing CAV1-mCherry (red channel) and Lamp1-EGFP (green channel) were mounted in a live cell chamber. FA was added to final 4% at t = 0 s, and time-lapse imaging was performed on an epifluorescence microscope at 0.2 Hz. Note the disappearance of CAV1-mCherry from numerous endosomal structures within the initial minutes of fixation (red circles), leaving empty Lamp1-EGFP organelles behind. Video is displayed at 10× real time.

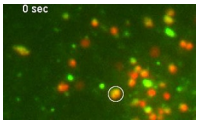

Video 3. **Targeting of CAV1 to the acidic lumen of endosomes.** CV1 cells coexpressing CAV1-mEGFP and CAV1-mCherry (12 h) were imaged on an epifluorescence setup equipped with a dual-view beam splitter at 0.2 Hz. The endosome marked by a circle is both red and green initially but loses green fluorescence as the endosome progresses toward the perinuclear area. Because mEGFP fluorescence is sensitive toward acidic pH, the loss of mEGFP fluorescence is consistent with targeting of CAV1 to the acidic lumen of LE/LYS (Fig. 5). Video is displayed at 50× real time.